This is the peer-reviewed, final accepted version for American Mineralogist, published by the Mineralogical Society of America.
The published version is subject to change. Cite as Authors (Year) Title. American Mineralogist, in press.
DOI: https://doi.org/10.2138/am-2021-7538. http://www.minsocam.org/

Revision 5. Crystal chemistry and high-temperature vibrational spectra of humite and norbergite: fluorine and titanium in humite-group minerals

Dan Liu[1], Sarah M. Hirner[2], Joseph R. Smyth[2], Junfeng Zhang[1,3], Xiaochao Shi[1], Xiang Wang[1], Xi Zhu[1], Yu Ye[1]*

[1]State Key Laboratory of Geological Processes and Mineral Resources, China University of Geosciences, Wuhan, 430074, China

[2]Department of Geological Sciences, University of Colorado, Boulder, Colorado, 80309, USA

[3]School of Earth Sciences, China University of Geosciences, Wuhan, 430074, China

*Contacting email: yeyu@cug.edu.cn

Always consult and cite the final, published document. See http:/www.minsocam.org or GeoscienceWorld

This is the peer-reviewed, final accepted version for American Mineralogist, published by the Mineralogical Society of America.
The published version is subject to change. Cite as Authors (Year) Title. American Mineralogist, in press.
DOI: https://doi.org/10.2138/am-2021-7538. http://www.minsocam.org/

Abstract

The humite-group minerals on the brucite-olivine join may be important dense hydrous magnesium silicate (DHMS) phases in the subducting slab. Fluorine and titanium can be incorporated into the crystal structures through the substitution mechanisms $(OH)^- = F^-$ and $Mg^{2+} + 2(OH)^- = Ti^{4+} + 2O^{2-}$. These substitutions have significant effects on the hydrogen bonding behavior in their crystal structures. Crystal structure refinements and *in situ* high-temperature Raman and Fourier transform infrared (FTIR) measurements were conducted on natural humite and norbergite crystals. Both minerals crystallize in space group *Pbnm*, and the isobaric Grüneisen parameters for the lattice and SiO_4 internal vibrations are compared with those of chondrodite, clinohumite, brucite and forsterite. For the humite-group minerals, the OH-stretching modes above 3450 cm^{-1} are affected by local H-H repulsion, whereas the behavior of those below 3450 cm^{-1} can be explained by F^- and Ti^{4+} substitutions, either of which may relieve the H-H repulsion effect. The Raman-active OH bands below 3450 cm^{-1} are affected by Ti^{4+} substitution, while the IR-active bands can be affected by either F^- or Ti^{4+} substitutions. Based on an analysis of the high-*T* Raman and FTIR spectra, the OH vibrations above and below 3450 cm^{-1} behave differently as a function of temperature, and similar behavior has also been observed for other dense hydrous silicate phases in the hydrous peridotite system. Hence, the lengths of the oxygen-oxygen edges in MgO_6 octahedra where protonation can occur become similar to each other at elevated temperatures. This may provide an

Always consult and cite the final, published document. See http:/www.minsocam.org or GeoscienceWorld

This is the peer-reviewed, final accepted version for American Mineralogist, published by the Mineralogical Society of America.
The published version is subject to change. Cite as Authors (Year) Title. American Mineralogist, in press.
DOI: https://doi.org/10.2138/am-2021-7538. http://www.minsocam.org/

atomistic explanation for the electrical conductivity properties of DHMS phases at high temperatures.

Keywords: humite-group minerals; Raman spectroscopy; high-temperature FTIR; OH-stretching mode; DHMS phases

Always consult and cite the final, published document. See http:/www.minsocam.org or GeoscienceWorld

This is the peer-reviewed, final accepted version for American Mineralogist, published by the Mineralogical Society of America.
The published version is subject to change. Cite as Authors (Year) Title. American Mineralogist, in press.
DOI: https://doi.org/10.2138/am-2021-7538. http://www.minsocam.org/

Introduction

Among various hydrous minerals, the humite-group minerals on the brucite (Bru)-olivine (Ol) join have been proposed as potential carriers of H_2O into the deep Earth and water reservoirs in the subduction zones and upper mantle under very hydrous compositions in the pressure range below 15 GPa (Kanzaki 1991 and 2016; Wunder et al. 1995; Wunder 1998; Berry and James 2001; Stalder and Ulmer 2001; Friedrich et al. 2002; Shen et al. 2015; Grützner et al. 2017b). These humite-group minerals along the Bru-Ol join include norbergite (1 Bru + 1 Ol), chondrodite (1 Bru + 2 Ol), humite (1 Bru + 3 Ol), clinohumite (1 Bru + 4 Ol). Chondrodite, clinohumite and phase A (3 Bru + 2 Ol) have been observed as the dehydration products of serpentine-group minerals in subducting slabs below 15 GPa (e.g., Stalder and Ulmer 2001; Smyth et al. 2006). The humite crystal structures closely resemble that of olivine, with zigzag chains of edge-sharing MO_6 octahedra linked by SiO_4 tetrahedra along the *c* axis (Gibbs and Ribbe et al. 1969; Jones et al. 1969; Gibbs et al. 1970; Ribbe and Gibbs 1971). Chondrodite and clinohumite crystallize in the space group $P2_1/b$, whereas the structures of norbergite and humite belong to the space group *Pbnm*, which is the same as that of olivine.

On the other hand, the elements fluorine and titanium are readily incorporated into the lattices of the humite-group minerals by the substitutions $(OH)^- = F^-$ (McDonough and Sun 1995) and $Mg^{2+} + 2(OH)^- = Ti^{4+} + 2O^{2-}$, respectively. Fluorine

Always consult and cite the final, published document. See http:/www.minsocam.org or GeoscienceWorld

This is the peer-reviewed, final accepted version for American Mineralogist, published by the Mineralogical Society of America.
The published version is subject to change. Cite as Authors (Year) Title. American Mineralogist, in press.
DOI: https://doi.org/10.2138/am-2021-7538. http://www.minsocam.org/

is an important halogen element (McDonough and Sun 1995) in the deep Earth due to its high volatility and incompatibility (Klemme and Stalder 2018). Due to the similar ionic radii between F^- (1.33 Å) and O^{2-} (1.40 Å) (Shannon 1976), fluorine can be incorporated into crystal structures along with hydroxyl groups in hydrous silicate minerals, such as amphibole, mica, apatite (Smith et al. 1981), humite-group minerals and nominally anhydrous minerals (NAMs), such as olivine, pyroxene and pyrope (Grützner et al. 2017a; Mosenfelder and Rossman 2013a, 2013b; Bernini et al. 2013). Fluorine has a significant effect on the properties of hydrous minerals under high-*P,T* conditions, such as the chemical stability (Grützner et al. 2017b) and electrical conductivity (Li et al. 2017). In addition, Ti-rich humite-group minerals are known from meta-basalts and hydrothermally altered peridotites. Therefore, studying the effects of Ti on the physical and chemical properties of these hydrous phases may provide a new understanding of the role of titanium in water recycling in the crust-mantle system (Scambelluri and Rampone 1999; Scambelluri and Philippot 2001; Shen et al. 2015; Qin et al. 2017).

In this study, we conducted *in situ* high-temperature Raman and Fourier transform infrared measurements on natural humite and norbergite samples. Combined with the previous high-temperature vibrational spectral studies of chondrodite and clinohumite (Lin et al. 1999 and 2000; Liu et al. 2019a), we can systematically examine the effects of F^- and Ti^{4+} substitutions on hydrogen bonds at high temperatures, which may provide a potential microscopic explanation for the

Always consult and cite the final, published document. See http:/www.minsocam.org or GeoscienceWorld

This is the peer-reviewed, final accepted version for American Mineralogist, published by the Mineralogical Society of America.
The published version is subject to change. Cite as Authors (Year) Title. American Mineralogist, in press.
DOI: https://doi.org/10.2138/am-2021-7538. http://www.minsocam.org/

effects of F and Ti on the stability of humite-group minerals under high-*P* and *T* conditions. We also comprehensively compared the temperature dependences of the OH bands in the DHMS phases in the hydrous peridotite system and the variations of the protonated O...O distances at elevated temperatures, which may be relevant to the high-temperature electrical conductivities of hydrous minerals (Guo and Yoshino 2013).

Samples and Experimental Methods

Sample composition

The norbergite sample with a pale orange color was collected in Franklin, New Jersey, U.S.A., where it coexists with calcite. The humite sample with a dark orange color was found in the Tilly Forster mine in Brewster, New York, U.S.A., which is a magnetite deposit occurring in marble (Buddington 1966). Sample chips were mounted in epoxy, and the top faces were polished for chemical analysis by electron microprobe. The compositions were analyzed with a JEOL 8600 SuperProbe operating at an accelerating voltage of 15 kV and a beam current of 20 nA, with a beam size of 5 μm. The selected certified mineral standards were olivine for Mg, Fe and Si; garnet for Mn; ilmenite for Ti; and topaz for F. At least 8 points were measured at different locations for each sample.

Always consult and cite the final, published document. See http:/www.minsocam.org or GeoscienceWorld

This is the peer-reviewed, final accepted version for American Mineralogist, published by the Mineralogical Society of America.
The published version is subject to change. Cite as Authors (Year) Title. American Mineralogist, in press.
DOI: https://doi.org/10.2138/am-2021-7538. http://www.minsocam.org/

Single-crystal X-ray diffraction

Two single crystals of humite (approximately 100 × 90 × 80 μm^3) and norbergite (approximately 95 × 80 × 75 μm^3) were selected for X-ray diffraction under ambient condition. The unit-cell parameters were measured using a Bruker P4 four-circle single-crystal diffractometer with a dual scintillation point detector mounted on an 18-kw rotating anode X-ray generator at the University of Colorado. The Mo-anode X-ray source was operated at a voltage of 50 kV and a current of 250 mA, and the averaged Mo $K\alpha_1$-$K\alpha_2$ mixed characteristic wavelengths were calibrated to be 0.71073 Å by a nearly spherical single crystal of ruby.

Intensity data were collected using a Bruker APEX II CCD detector mounted on a P4 diffractometer. Intensities were measured with the 2θ scanning range up to 70° for norbergite and humite. Structure refinements were conducted using the program SHELX-97 (Sheldrick 2008) in the software package WinGX (Farrugia 2012), with the scattering factors of Mg^{2+}, Fe^{2+} and Si^{4+} from Cromer and Mann (1968) and that of O^{2-} from Tokonami (1965).

High-temperature Raman and FTIR spectra

Unpolarized Raman spectra were measured using a Horiba LabRAM HR Evolution system with a micro confocal Raman spectrometer. A green beam (λ = 532 nm, P = 20 mW and spot diameter approximately 1 μm) from a Nd YAG laser source

Always consult and cite the final, published document. See http:/www.minsocam.org or GeoscienceWorld

was used for excitation, and the Raman shift was calibrated using a Si single crystal. Two unoriented crystals of humite and norbergite (approximately 100×150×50 μm^3) were placed on a sapphire plate in a Linkam TS1500 heating stage. The backscattered spectra were collected in the Raman shift range of 100-4000 cm^{-1}, with a duration of 20 minutes and an accumulation of 3 times.

Unpolarized FTIR spectra were obtained from 3000 to 4000 cm^{-1} on a Nicolet iS50 FTIR spectrometer coupled with a continuυm microscope using a KBr beam-splitter and a liquid-nitrogen cooled MCT-A detector. Each spectrum was obtained in the wavenumber range of 3000-4000 cm^{-1} with a 100 × 100 μm^2 aperture, an accumulation of 128 scans and a resolution of 4 cm^{-1}. Unoriented crystals of humite and norbergite, with a thickness of approximately 40 to 50 μm, were mounted on a sapphire window of an Instec HS1300 heating stage. Background spectra were also collected at each step after the measurement of the sample.

For *in situ* high-temperature Raman and FTIR measurements, resistance heaters were used to produce high temperatures and the temperatures were automatically controlled by a commercial temperature-controlling unit with uncertainties of approximately 1 K. The samples were heated from 293 K to 993 K, with increments of 50 K and a heating rate of 20 K/min. At each step, the target temperature was held for at least 5 minutes for thermal equilibration before measurement. The sample chambers were filled with N_2 to avoid any potential oxidation at high temperatures.

Always consult and cite the final, published document. See http:/www.minsocam.org or GeoscienceWorld

This is the peer-reviewed, final accepted version for American Mineralogist, published by the Mineralogical Society of America.
The published version is subject to change. Cite as Authors (Year) Title. American Mineralogist, in press.
DOI: https://doi.org/10.2138/am-2021-7538. http://www.minsocam.org/

Another Raman/FTIR spectrum was taken when the sample was quenched to room temperature after heating. Peakfit v4.12 software was used to analyze both the Raman and infrared spectra.

Results

Compositions and crystal structures

The averaged oxide weights from EPMA measurements are listed in **Table 1**. The formulas can be expressed as $Mg_{6.50}Fe_{0.48}Ti_{0.016}Mn_{0.016}Si_{2.99}O_{12}F_{0.66}(OH)_{1.31}O_{0.03}$ for humite and $Mg_{2.97}Fe_{0.011}Ti_{0.025}Si_{0.99}O_4F_{1.23}(OH)_{0.72}O_{0.05}$ for norbergite. The water contents are 2.36 wt.% and 3.16 wt.%, respectively, while the F/(F+OH) ratios are 33% and 61% for humite and norbergite, respectively.

Both the humite (**Fig. 1a**) and norbergite (**Fig. 1b**) structures were refined in space group *Pbnm* (please refer to the deposited CIF files for details), which are consistent with the previous studies (Gibbs and Ribbe 1969; Ribbe and Gibbs 1971; Wunder et al. 1995; Cámara 1997; Kuribayashi et al. 2008). In the crystal structures of the humite-group minerals, the M3 sites are the preferred sites for Ti^{4+} substitution: $Mg^{2+} + 2(OH)^- = Ti^{4+} + 2O^{2-}$ (Robinson et al. 1973; Fujino and Takeuchi 1978; Ribbe 1979; Friedrich et al. 2001), whereas the oxygen sites of 'OH' are the preferred sites for protonation [$O^{2-} + H^+ = (OH)^-$] and F^- substitution [$(OH)^- = F^-$] (Gibbs and Ribbe 1969; Ribbe and Gibbs 1971; Kuribayashi et al. 2008). Protonation typically happens

Always consult and cite the final, published document. See http:/www.minsocam.org or GeoscienceWorld

This is the peer-reviewed, final accepted version for American Mineralogist, published by the Mineralogical Society of America.
The published version is subject to change. Cite as Authors (Year) Title. American Mineralogist, in press.
DOI: https://doi.org/10.2138/am-2021-7538. http://www.minsocam.org/

along the OH...OH edges of $Mg(O,OH)_6$ octahedra, where 'OH' in the item of 'OH…OH edge' stands for an oxygen site, and the neighboring H-H repulsion in the local lattice structure is illustrated in **Fig. 1(c,d)**, which will be discussed in more details in the following FTIR measurements. As estimated from the structure refinement in this study, the orientation of the O-H bond deflects approximately 15° away from the OH…OH edge, and the angle of the O-H…O bonds is 160°, which is consistent with the angles reported for other humite-group minerals in the range of 160 to 170° (Cámara 1997; Berry and James 2001; Friedrich et al. 2001). The nonlinear O-H…O bonds are related to the neighboring H-H repulsion, which is discussed more in the following.

In addition, the OH-related M-O bond lengths (M25-OH in humite; M2-OH and M3-OH in norbergite) are generally shorter than the others due to F^- substitution. Similar behaviors have also been reported for chondrodite (Ye et al. 2015) and clinohumite (Ye et al. 2013). The MO_6 octahedral volumes decrease in the order M2 > M25 > M1 > M3 for humite and M2 > M3 for norbergite. The SiO_4 tetrahedral volumes of this humite sample are slightly smaller than those in norbergite, clinohumite and chondrodite.

High-temperature vibrational spectra

We conducted high-temperature Raman measurements on the lattice (< 1000

Always consult and cite the final, published document. See http:/www.minsocam.org or GeoscienceWorld

cm^{-1}) and OH-stretching (3000 - 4000 cm^{-1}) vibrations for both humite and norbergite. Selected Raman spectra for the lattice modes at various temperatures are shown in **Fig. 2(a, b)**; and the fitted peak positions at ambient temperature are listed in **Appendix Table 1.** Our spectra measured at room temperature are consistent with those from previous studies (Frost et al. 2007; Palmer et al. 2007). Distinct internal Si-O stretching modes were detected at 843 (most intense), 863, 931 and 967 cm^{-1} for humite and at 851 (most intense), 884, 894, 951 and 973 cm^{-1} for norbergite at ambient temperature.

Most of the Raman bands remain sharp and distinguishable throughout the experimental temperature range. The modes shift systematically to lower frequencies at elevated temperatures. The variations in the frequencies for these modes with temperature are plotted in **Fig. 3(a,b)**, and the fitted slopes $(\partial v_i/\partial T)_P$ are listed in **Appendix Table 1**. The temperature dependences of these Raman-active modes typically vary from -0.01 to -0.03 $cm^{-1}\cdot K^{-1}$ for most of the vibrations except for the case of $MgOH/M^{2+}OH$ deformations, which show temperature dependences in the range of 0 to -0.01 $cm^{-1}\cdot K^{-1}$. Another Raman spectrum was acquired for each sample when it was quenched to room temperature, and no significant differences were observed between this spectrum and that obtained before heating, suggesting that these phases are stable without a noticeable phase transition or amorphization up to approximately 1000 K at ambient pressure in a N_2 atmosphere.

Always consult and cite the final, published document. See http:/www.minsocam.org or GeoscienceWorld

The Raman and FTIR spectra of the OH-stretching bands under ambient condition are compared in **Fig. 4** for the humite and norbergite samples from this study and the natural clinohumite sample from the study by Liu et al. (2019a). Two OH bands at 3310 and 3405 cm^{-1} were observed in the Raman spectrum for clinohumite, which are related to the presence of Ti^{4+} substitution (Frost et al. 2007; Koga et al. 2014). The Ti concentration in the natural clinohumite sample (C_{TiO2} = 3.10 wt.%) was significantly higher than the Ti concentrations of humite (C_{TiO2} = 0.26 wt.%) and norbergite (C_{TiO2} = 0.99 wt.%). An extremely weak OH-stretching mode at approximately 3390 cm^{-1} was detected in the Raman spectrum of the Ti-poor humite sample at room temperature. A very low signal-noise ratio was observed for the Raman spectra on the norbergite sample because the intensity of the OH band is much lower and the fluorescence background is much stronger, perhaps due to the high F^- concentration, compared with that of humite. Similar behaviors have also been reported based on the Raman spectra of F-rich natural norbergite samples (Liu et al. 1999).

High-temperature FTIR and Raman spectra were collected for both the humite and norbergite samples at temperatures up to 993 K, in the vibrational frequency range of 3000 – 4000 cm^{-1} (**Fig. 5**). These OH bands gradually became broader and weaker at elevated temperatures. The strong bands at approximately 3500 - 3600 cm^{-1} for humite could be distinguished at high temperatures, while the weak peak at 3318 cm^{-1} for norbergite overlapped greatly with the peak at 3365 cm^{-1} above 493 K. The

Always consult and cite the final, published document. See http:/www.minsocam.org or GeoscienceWorld

OH bands were recovered when the samples were quenched to room temperature, and the intensities of the OH absorbance bands in the range of 3200 - 3700 cm^{-1} remained similar to that before heating, suggesting no significant dehydration in these humite-group minerals at temperatures up to 993 K.

Discussion

OH-stretching bands and temperature dependence

The most intense OH bands were measured at 3558 and 3573 cm^{-1} for humite and at 3580 cm^{-1} for norbergite, corresponding to estimated O…O distances of 3.02 - 3.16 Å (Libowitzky 1999). These values are close to the measured oxygen-oxygen distances between two 'OH' sites for both humite (2.980(8) Å) (**Fig. 1c**) and norbergite (3.020(2) Å) (**Fig. 1d**) based on the single-crystal XRD data. The OH-stretching bands above 3450 cm^{-1}, corresponding to hydrogen bonds ($d_{H...O}$) longer than 2 Å (Libowitzky 1999), could be affected by neighboring H-H repulsion, as in the structure of chondrodite and clinohumite (e.g., Lin et al. 1999 and 2000; Liu et al. 2019a). The intensity of the Raman-active OH mode for norbergite at 3582 cm^{-1} is somewhat lower due to the higher F^- concentration (F/(F+OH) = 63%), and the fluorescence background is much stronger.

In contrast, additional OH-stretching bands were detected in the FTIR spectra (**Fig. 4**) at wavenumbers below 3450 cm^{-1} ($d_{H...O}$ < 2 Å) in natural humite-group

Always consult and cite the final, published document. See http:/www.minsocam.org or GeoscienceWorld

minerals (e.g., Kitamura et al. 1987; Miller et al. 1987; Williams 1992; Cynn et al. 1996; Kurosawa et al. 1997; Kuribayashi et al. 2004; Matsyuk and Langer 2004; Prasad and Sarma 2004; Berry et al. 2005; Shen et al. 2014; Liu et al. 2019a). These bands reflect the nature of the local OH…F and/or OH…O + Ti(M3) environments (e.g., Cynn et al. 1996; Kuribayashi et al. 2004; Shen et al. 2014; Liu et al. 2019a), according to the substitution mechanisms of $(OH)^- = F^-$ and $Mg^{2+} + 2(OH)^- = Ti^{4+} + 2O^{2-}$. Through such an exchanging mechanism, neighboring H-H repulsion could be relieved, resulting in OH-stretching bands at lower wavenumbers. Moreover, the O…O distance between two 'OH' sites refined from our single-crystal XRD datasets (2.782(4) Å for humite and 2.699(1) Å for norbergite) can be possible protonation sites for these OH bands and fit well with the correlation reported by Libowitzky (1999).

The variations in the frequencies of both the Raman- and IR-active OH bands with temperature are plotted in **Fig. 6**. The temperature derivatives, in the unit of $cm^{-1}\cdot K^{-1}$, are listed in **Appendix Table 2.** For both humite and norbergite, the OH bands above 3450 cm^{-1} all show negative temperature dependences, while the ones below 3450 cm^{-1} systematically exhibit positive temperature dependences. Similar behavior has been reported for natural clinohumite samples (Liu et al. 2019a). For the elongated hydrogen bonds above 3450 cm^{-1} in the humite-group minerals including norbergite, humite, chondrodite and clinohumite, the neighboring H-H repulsion force becomes weaker during thermal expansion of the crystal structure, and then the

Always consult and cite the final, published document. See http:/www.minsocam.org or GeoscienceWorld

This is the peer-reviewed, final accepted version for American Mineralogist, published by the Mineralogical Society of America.
The published version is subject to change. Cite as Authors (Year) Title. American Mineralogist, in press.
DOI: https://doi.org/10.2138/am-2021-7538. http://www.minsocam.org/

hydrogen bond gets shorter as the OH-stretching vibrations shift to lower frequencies (Lin et al. 2000; Liu et al. 1999; 2019a). However, without such a H-H repulsion effect, the hydrogen bonds below 3450 cm^{-1} would become longer at higher temperatures. The OH modes would subsequently shift to higher frequencies, which is common in most hydrous minerals.

The temperature dependences of the OH-stretching modes, $(\partial v_i/\partial T)_P$, for humite-group minerals are compared with other dense hydrous Mg-silicate minerals in the peridotite system (MgO-SiO_2-$Mg(OH)_2$) (**Fig. 7**), such as serpentine, brucite, talc, phases A, B, E and super hydrous phase B (Liu et al. 1997a, 1997b, 1998, 1999 and 2002; Lin et al. 1999 and 2000; Zhang et al. 2006; Trittschack et al. 2012; Liu et al. 2019a and 2019b; Zhu et al. 2019; this study). The OH bands above 3450 cm^{-1} typically show a negative temperature dependence, whereas those below 3450 cm^{-1} typically exhibit a positive temperature dependence. A similar behavior was also observed for NAMs with hydrogen defects, such as in clinopyroxene-group minerals (Yang et al. 2019). Hydrogen bond lengths and the lengths of the O...O edges where protonation occurs are positively correlated with the frequencies of the OH-stretching modes for hydrous minerals (Libowitzky 1999). Hence, the O…O distances for protonation in these DHMS phases have a tendency to become similar to each other at elevated temperatures.

Always consult and cite the final, published document. See http:/www.minsocam.org or GeoscienceWorld

F^- and Ti^{4+} substitutions in humite-group minerals

Fluorine and titanium can be incorporated into humite-group phases, which has a significant effect on the OH-stretching behavior. Here, we analyzed the reported Raman and infrared spectra of humite-group minerals with various F^- and Ti^{4+} concentrations (**Appendix Table 3**) and integrated the intensities of the OH-stretching bands in the frequency ranges below and above 3450 cm^{-1} ($I_{<3450}$ and $I_{>3450}$, respectively) for each sample. We also calculated the F^- (X_F = F/(F+OH)) and Ti^{4+} contents at the M3 sites (X_{Ti} = Ti/(Mg+Fe-n×Si), n = 4 for clinohumite, 3 for humite, 2 for chondrodite and 1 for norbergite).

The $I_{<3450}$: $I_{>3450}$ intensity ratios of the IR-active OH-stretching modes generally increase with the F^- concentration **(Fig. 8a)** for samples with compositions $X_F \geq 0.33$ and $X_{Ti} \leq 0.03$ (Williams 1992; Cynn et al. 1996; Kuribayashi et al. 2004; This study). It is noted that Hughes and Pawley (2019) did not observe any Raman-active modes below 3450 cm^{-1} for synthetic Ti-free humite-group minerals ($0.15 < X_F < 0.6$). In contrast, for samples with relatively high Ti^{4+} ($X_{Ti} \geq 0.08$) and low F^- ($X_F \leq 0.17$) contents, both the FTIR **(Fig. 8b)** and Raman **(Fig. 8c)** measurements show a general trend where the $I_{<3450}$: $I_{>3450}$ ratios increase as the Ti^{4+} concentration increases (Frost et al. 2007; Ye et al. 2013, 2015; Koga et al. 2014; Shen et al. 2014; Liu et al. 2019a; This study).

Hence, below 3450 cm^{-1}, the Raman-active OH-stretching modes can be affected

Always consult and cite the final, published document. See http:/www.minsocam.org or GeoscienceWorld

only by Ti^{4+} substitution, while the IR-active modes may be generated by either F^- or Ti^{4+} substitution, with Ti^{4+} substitution possibly playing a more important role than F^- substitution. Both substitutions could relieve the adjacent H-H repulsion effect and make the neighboring hydrogen bonds shorter and stronger, with the OH-stretching modes shifting to lower wavenumbers. These observations may also provide a reasonable explanation for the absence of OH-pure humite minerals in nature (Fujino and Takeuchi 1978). In addition, high-*P,T* experiments have revealed that F^- substitution could significantly stabilize hydrous minerals at higher temperatures, such as amphibole (Foley 1991), talc (Rywak and Burlitch 1996) and clinohumite (Grützner et al. 2017a).

Isobaric Grüneisen parameters

The isobaric Grüneisen parameter, γ_{iP}, is used to measure the temperature effect on vibrational frequencies (i.e., Gillet et al. 1991; Okada et al. 2008; Yang et al. 2015; Liu et al. 2019a):

$$\gamma_{ip} = \left(\frac{\partial ln v_i}{\partial \rho}\right)_P = -\frac{1}{\alpha v_{0i}}\left(\frac{\partial v_i}{\partial T}\right)_P \quad (1)$$

where υ_{0i} is the mode frequency under ambient condition, $(\partial v_i/\partial T)_P$ is the temperature derivative of the frequency and α is the averaged thermal expansion coefficient. Ye et al. (2013) reported an empirical relationship between the averaged volumetric thermal expansion coefficient (α_0, $10^{-6}\cdot K^{-1}$) and density (ρ, g/cm^3) for the humite-group

Always consult and cite the final, published document. See http:/www.minsocam.org or GeoscienceWorld

minerals on the brucite-olivine join: $\alpha_0 = 156(7) - 37(2) \times \rho$, and Ye et al. (2015) also reported a systematic relationship between α_0 and the water concentration (C_{H2O}, wt.%): $\alpha_0 = 35.3(4) + 1.02(3) \times C_{H2O}$. Based on the densities and the water contents of humite ($\rho = 3.222$ g/cm^3, $C_{H2O} = 2.36$ wt.%) and norbergite ($\rho = 3.143$ g/cm^3, $C_{H2O} = 3.16$ wt.%), we estimated average α_0 values of 37.2(9) $\times 10^{-6}$ K^{-1} for humite and 39.1(7) $\times 10^{-6}$ K^{-1} for norbergite, and calculated the isobaric Grüneisen parameters for both the lattice vibrations and OH-stretching modes (**Appendix Tables 1 and 2**).

The vibrational modes of the humite minerals are divided into five regions (Lin et al. 2000; Liu et al. 1999; Mernagh et al. 1999; Grützner et al. 2017b): (1) MO_6 octahedral vibrations below 350 cm^{-1}; (2) SiO_4 internal bending modes from 350 to 750 cm^{-1}; (3) vibrations associated with MgOH and other $M^{2+}OH$ deformations from 740 to 790 cm^{-1}; (4) SiO_4 internal stretching modes from 800 to 1000 cm^{-1}; and (5) internal OH-stretching modes from 3000 to 4000 cm^{-1}. The calculated isobaric Grüneisen parameters for the DHMS phases on the brucite-olivine join are compared in **Fig. 9**, including brucite (Zhu et al. 2019), norbergite (this study), chondrodite (Mernagh et al. 1999), humite (this study), clinohumite (Liu et al. 2019a) and forsterite (Gillet et al. 1991). For the lattice vibrational modes below 1000 cm^{-1}, the humite-group minerals, including norbergite, chondrodite, humite and clinohumite, show isobaric Grüneisen parameters with similar values, compared with those for forsterite. The γ_{iP} parameters range from 0.93 to 3.2 for the MO_6 vibrations, 0.27 to 2.5 for the SiO_4 bending modes, 0.19 to 1.3 for the SiO_4 stretching modes and -0.22 to

Always consult and cite the final, published document. See http:/www.minsocam.org or GeoscienceWorld

This is the peer-reviewed, final accepted version for American Mineralogist, published by the Mineralogical Society of America.
The published version is subject to change. Cite as Authors (Year) Title. American Mineralogist, in press.
DOI: https://doi.org/10.2138/am-2021-7538. http://www.minsocam.org/

0.36 for the OH-stretching modes. The γ_{iP} parameters of the OH-stretching modes above 3000 cm^{-1} are typically smaller in magnitude than those for the lattice vibrations due to the higher frequencies, although their temperature dependences, $(\partial v_i/\partial T)_P$, are similar.

Implications

Both the Raman and FTIR spectra of nominally hydrous minerals indicate that the hydrogen bond lengths and the O…O distances for protonation are more similar to each other at high temperatures, as compared with the case at room temperature. During such a gradual changing process without significant dehydration, the protons might have similar mobility at high temperatures, as is the case for hydrous clinopyroxenes (Yang et al. 2019). Variations in the local environments around the protons may be important for understanding the electric conduction mechanism in these DHMS phases at high temperatures.

The experiments reveal that the electrical conductivity is generally independent of the water concentrations in hydrous minerals, including talc, serpentine, brucite, phase A, superhydrous phase B and phengite, (Guo et al. 2011; Guo and Yoshino 2013, 2014; Chen et al. 2018). The low activation enthalpies for conductivity (< 0.83 eV) in these hydrous phases indicate that the conduction mechanism should be attributed to the migration of hydrogen (proton conduction). However, an enthalpy as large as 1.5

Always consult and cite the final, published document. See http:/www.minsocam.org or GeoscienceWorld

eV is required to break the covalent O-H bands down and generate interstitial H^+ and H^+-related vacancies in the lattice structure (intrinsic mechanism). Then, the formation of O^{2-} due to impurities in the crystal structure is proposed as an extrinsic mechanism, in which protons (H^+) dominantly transfer through hydrogen-bond interactions between extrinsic O^{2-} and neighboring $(OH)^-$ (Guo and Yoshino 2013). In this case, the potential energy of H^+ migration from OH^- donors to adjacent O^{2-} acceptors is closely related to the O…O distance, as well as the lattice conductivity in hydrous minerals.

Electrical conductivity measurements on F-bearing phlogopite (Li et al. 2017) show that F conduction should be more important than OH conduction in phlogopite above 900 K. Hence, more high-*P,T* experiments on the effects of F and Ti on the electrical conductivities of various DHMS phases, including the humite-group minerals, are necessary to elucidate the complex electrical conductivity behaviors in subduction zones.

Acknowledgments

This study was supported by three grants from the National Natural Science Foundation of China (Grant Nos. 41590621 and 41672041), the US National Science Foundation (Grant EAR14-16979 to JRS) and the Fundamental Research Funds for National Universities, China University of Geosciences (Wuhan). The single-crystal

Always consult and cite the final, published document. See http:/www.minsocam.org or GeoscienceWorld

This is the peer-reviewed, final accepted version for American Mineralogist, published by the Mineralogical Society of America.
The published version is subject to change. Cite as Authors (Year) Title. American Mineralogist, in press.
DOI: https://doi.org/10.2138/am-2021-7538. http://www.minsocam.org/

X-ray diffraction was carried out at the University of Colorado, and the Raman and FTIR spectra were collected at China University of Geosciences (Wuhan).

Always consult and cite the final, published document. See http:/www.minsocam.org or GeoscienceWorld

This is the peer-reviewed, final accepted version for American Mineralogist, published by the Mineralogical Society of America.
The published version is subject to change. Cite as Authors (Year) Title. American Mineralogist, in press.
DOI: https://doi.org/10.2138/am-2021-7538. http://www.minsocam.org/

References

Bernini, D., Wiedenbeck, M., Dolejš, D., and Keppler, H. (2013) Partitioning of halogens between mantle minerals and aqueous fluids: implications for the fluid flow regime in subduction zones. Contributions to Mineralogy and Petrology, 165, 117-128.

Berry, A.J., and James, M. (2001) Refinement of hydrogen positions in synthetic hydroxyl-clinohumite by powder neutron diffraction. American Mineralogist, 86, 181-184.

Berry, A.J., Hermann, J., O'Neill, H.S.C., and Foran, G.J. (2005) Fingerprinting the water site in mantle olivine. Geology, 33, 869-872.

Buddington, A.F. (1966) The Precambrian magnetite deposits of New York and New Jersey. Economic Geology, 61, 484-510.

Cámara, F. (1997) New data on the structure of norbergite: location of hydrogen by X-ray diffraction. Canadian Mineralogist, 35, 1523-1530.

Chen, S., Guo, X., Yoshino, T., Jin, Z., and Li, P. (2018) Dehydration of phengite inferred by electrial conductivity measurements: Implication for the high conductivity anomalies relevant to the subduction zones. Geology, 46, 11-14.

Cromer, D.T., and Mann, J.B. (1968) X-ray scattering factors computed from numerical Hartree-Fock wave functions. Acta Crystallographica, A24, 321-324.

Always consult and cite the final, published document. See http:/www.minsocam.org or GeoscienceWorld

This is the peer-reviewed, final accepted version for American Mineralogist, published by the Mineralogical Society of America.
The published version is subject to change. Cite as Authors (Year) Title. American Mineralogist, in press.
DOI: https://doi.org/10.2138/am-2021-7538. http://www.minsocam.org/

Cynn, H., Hofmeister, A.M., Burnley, P.C., and Navrotsky, A. (1996) Thermodynamic properties and hydrogen bonding speciation from vibrational spectra of dense hydrous magnesium silicates. Physics and Chemistry of Minerals, 23, 361-376.

Farrugia, L.J. (2012) WinGX and ORTEP for Windows: an update. Journal of Applied Crystallography, 45, 849-854.

Foley, S. (1991) High-pressure stability of the fluor- and hydroxy-endmembers of pargasite and K-richterite. Geochimica et Cosmochimica Acta, 55, 2689-2694.

Friedrich, A., Lager, G.A., Kunz, M., Chakoumakos, B.C., Smyth, J.R., and Schultz, A.J. (2001) Temperature-dependent single-crystal neutron diffraction study of natural chondrodite and clinohumites. American Mineralogist, 86, 981-989.

Friedrich, A., Lager, G.A., Ulmer, P., Kunz, M., and Marshall, W.G. (2002) High-pressure single-crystal X-ray and powder neutron study of F, OH/OD-chondrodite: Compressibility, structure, and hydrogen bonding. American Mineralogist, 87, 931-939.

Frost, R.L., Palmer, S.J., Bouzaid, J.M., and Jagannadha Reddy, B. (2007) A Raman spectroscopic study of humite minerals. Journal of Raman Spectroscopy, 38, 68-77.

Fujino, K., and Takéuchi, Y. (1978) Crystal chemistry of titanian chondrodite and

Always consult and cite the final, published document. See http:/www.minsocam.org or GeoscienceWorld

This is the peer-reviewed, final accepted version for American Mineralogist, published by the Mineralogical Society of America.
The published version is subject to change. Cite as Authors (Year) Title. American Mineralogist, in press.
DOI: https://doi.org/10.2138/am-2021-7538. http://www.minsocam.org/

titanian clinohumite of high-pressure origin. American Mineralogist, 63, 535-543.

Gibbs, G.V., and Ribbe, P.H. (1969) The crystal structures of the humite minerals: I. Norbergite. American Mineralogist, 54, 376-390.

Gibbs, G.V., Ribbe, P.H., and Anderson, C.P. (1970) The crystal structures of the humite minerals. II. Chondrodite. American Mineralogist, 55, 1182-1194.

Gillet, P., Richet, P., Guyot, F., and Fiquet, G. (1991) High-temperature thermodynamic properties of forsterite. Journal of Geophysical Research, 96, 11805-11816.

Grützner, T., Kohn, S.C., Bromiley, D.W., Rohrbach, A., Berndt, J., and Klemme, S. (2017a) The storage capacity of fluorine in olivine and pyroxene under upper mantle conditions. Geochimica et Cosmochimica Acta, 208, 160-170.

Grützner, T., Klemme, S., Rohrbach, A., Gervasoni, F., and Berndt, J. (2017b) The role of F-clinohumite in volatile recycling processes in subduction zones. Geology, 45, 443-446.

Guo, X., and Yoshino, T. (2013) Electrical conductivity of dense hydrous magnesium silicates with implication for conductivity in the stagnant slab. Earth and Planetary Science Letters, 369-370, 239-247.

Guo, X., and Yoshino, T. (2014) Pressure-induced enhancement of proton conduction

Always consult and cite the final, published document. See http:/www.minsocam.org or GeoscienceWorld

This is the peer-reviewed, final accepted version for American Mineralogist, published by the Mineralogical Society of America.
The published version is subject to change. Cite as Authors (Year) Title. American Mineralogist, in press.
DOI: https://doi.org/10.2138/am-2021-7538. http://www.minsocam.org/

in brucite. Geophysical Research Letters, 41, 813-819.

Guo, X., Yoshino, T., and Katayama, I. (2011) Electrical conductivity anisotropy of deformed talc rocks and serpentinites at 3 GPa. Physics Earth and Planetary Interiors, 188, 69-81.

Hughes, L., and Pawley, A. (2019) Fluorine partitioning between humite-group minerals and aqueous fluids: implications for volatile storage in the upper mantle. Contributions to Mineralogy and Petrology, 174, 78, doi: 10.1007/s00410-019-1614-2

Jones, N.W., Ribbe, P.H., and Gibbs, G.V. (1969) Crystal chemistry of the humite minerals. American Mineralogist, 54, 391-411.

Kanzaki, M. (1991) Stability of hydrous magnesium silicates in the mantle transition zone. Physics of the Earth and Planetary Interiors, 66, 307-312.

Kanzaki, M. (2016) Hydrogen distribution in chondrodite: a first-principles calculation. Journal of Mineralogical and Petrological Sciences, 111, 425-430.

Kitamura, M., Kondoh, S., Morimoto, N., Miller, G.H., Rossman, G.R., and Putnis, A. (1987) Planar OH-bearing effects in mantle olivine. Nature, 328, 143-145.

Klemme, S., and Stalder, R. (2018) Halogens in the Earth's mantle: what we know and what we don't. In Harlov, D.E., Aranovich, L. (Eds.). The role of hydrogens in Terrestrial and Extraterrestrial Geochemical Processes: Surface, Crust, and

Always consult and cite the final, published document. See http:/www.minsocam.org or GeoscienceWorld

This is the peer-reviewed, final accepted version for American Mineralogist, published by the Mineralogical Society of America.
The published version is subject to change. Cite as Authors (Year) Title. American Mineralogist, in press.
DOI: https://doi.org/10.2138/am-2021-7538. http://www.minsocam.org/

Mantle., p. 847-869. Springer International Publishing, Berlin.

Koga, K.T., Garrido, C.J., Padrón-Navarta, J.A., Sánchez-Vizcaíno, V.L., and Gómez-Pugnaire, M.T. (2014) FTIR and Raman spectroscopy characterization of fluorine-bearing titanian clinohumite in antigorite serpentinite and chlorite harzburgite. Earth Planets and Space, 66, 60, doi: 10.1186/1880-5981-66-60

Kuribayashi, T., Kagi, H., Tanaka, M., Akizuki, M., and Kudoh, Y. (2004) High-pressure single-crystal X-ray diffraction and FT-IR observation of natural chondrodite and synthetic OH-chondrodite. Journal of Mineralogical and Petrological Sciences, 99, 118-129.

Kuribayashi, T., Tanaka, M., and Kudoh, Y. (2008) Synchrotron, X-ray analysis of norbergite, $Mg_{2.98}Fe_{0.001}Ti_{0.02}Si_{0.99}O_4(OH)_{0.31}F_{1.69}$ structure at high pressure up to 8.2 GPa. Physics and Chemistry of Minerals, 35, 559-568.

Kurosawa, M., Yurimoto, H., and Sueno, S. (1997) Patterns in the hydrogen and trace element compositions of mantle olivines. Physics and Chemistry of Minerals, 24, 385-395.

Li, Y., Jiang, H., and Yang, X. (2017) Fluorine follows water: Effect on electrical conductivity of silicate minerals by experimental constraints from phlogopite. Geochimica et Cosmochimica Acta, 217, 16-27.

Libowitzky, E. (1999) Correlation of O-H stretching frequencies and O-H...O

Always consult and cite the final, published document. See http:/www.minsocam.org or GeoscienceWorld

This is the peer-reviewed, final accepted version for American Mineralogist, published by the Mineralogical Society of America.
The published version is subject to change. Cite as Authors (Year) Title. American Mineralogist, in press.
DOI: https://doi.org/10.2138/am-2021-7538. http://www.minsocam.org/

hydrogen bond lengths in minerals. Monatshefte für Chemie, 130, 1047-1059.

Lin, C.C., Liu, L.G., and Irifune, T. (1999) High-pressure Raman spectroscopic study of chondrodite. Physics and Chemistry of Minerals, 26, 226-233.

Lin, C.C., Liu, L.G., Mernagh, T.P., and Irifune, T. (2000) Raman spectroscopic study of hydroxyl-clinohumite at various pressures and temperatures. Physics and Chemistry of Minerals, 27, 320-331.

Liu, L.G., Mernagh, T.P., Lin, C.C., and Irifune, T. (1997a) Raman spectra of phase E at various pressures and temperatures with geophysical implications. Earth and Planetary Science Letters, 149, 57-65.

Liu, L.G., Lin, C.C., Mernagh, T.P., and Irifune, T. (1997b) Raman spectra of phase A at various pressures and temperatures. Journal of Physics and Chemistry of Solids, 58, 2023-2030.

--- (1998) Raman spectra of phase B at various pressures and temperatures. Journal of Physics and Chemistry of Solids, 59, 871-877.

Liu, L.G., Lin, C.C., and Mernagh, T.P. (1999) Raman spectra of norbergite at various pressures and temperatures. European Journal of Mineralogy, 11, 1011-1021.

Liu, L.G., Lin, C.C., Mernagh, T.P., and Inoue T. (2002) Raman spectra of phase C (superhydrous phase B) at various pressures and temperatures. European Journal of Mineralogy, 14, 15-23.

Always consult and cite the final, published document. See http:/www.minsocam.org or GeoscienceWorld

This is the peer-reviewed, final accepted version for American Mineralogist, published by the Mineralogical Society of America.
The published version is subject to change. Cite as Authors (Year) Title. American Mineralogist, in press.
DOI: https://doi.org/10.2138/am-2021-7538. http://www.minsocam.org/

Liu, D., Pang, Y.Y., Ye, Y., Jin, Z.M., Smyth, J.R., Yang, Y., Zhang, Z.M., and Wang, Z.P. (2019a) In-situ high-temperature vibrational spectra for synthetic and natural clinohumite: Implications for dense hydrous magnesium silicates in subduction zones. American Mineralogist, 104, 53-63.

Liu, D., Wang, S., Smyth, J.R., Zhang, J., Wang, X., Zhu, X., and Ye, Y. (2019b) In situ infrared spectra for hydrous forsterite up to 1243 K: hydration effect on thermodynamic properties. Minerals, 9, 512, doi: 10.3390/min9090512

Matsyuk, S.S., and Langer, K. (2004) Hydroxyl in olivines from mantle xenoliths in kimberlites of the Siberian platform. Contributions to Mineralogy and Petrology, 147, 413-437.

McDonough, W.F., and Sun, S. (1995) The composition of the Earth. Chemical Geology, 120, 223-253.

Mernagh, T.P., Liu, L.G., and Lin, C.C. (1999) Raman spectra of chondrodite at various temperatures. Journal of Raman Spectroscopy, 30, 963-969.

Miller, G.H., Rossman, G.R., and Harlow, G.E. (1987) The natural occurrence of hydroxide in olivine. Physics and Chemistry of Minerals, 14, 461-472.

Mosenfelder, J.L., and Rossman, G.R. (2013a) Analysis of hydrogen and fluorine in pyroxenes: I. Orthopyroxene. American Mineralogist, 98, 1026-1041.

Mosenfelder, J.L., and Rossman, G.R. (2013b) Analysis of hydrogen and fluorine in

Always consult and cite the final, published document. See http:/www.minsocam.org or GeoscienceWorld

This is the peer-reviewed, final accepted version for American Mineralogist, published by the Mineralogical Society of America.
The published version is subject to change. Cite as Authors (Year) Title. American Mineralogist, in press.
DOI: https://doi.org/10.2138/am-2021-7538. http://www.minsocam.org/

pyroxenes: II. Clinopyroxene. American Mineralogist, 98, 1042-1054.

Okada, T., Narita, T., Nagai, T., and Yamanaka, T. (2008) Comparative Raman spectroscopic study on ilmenite-type $MgSiO_3$ (akimotoite), $MgGeO_3$, and $MgTiO_3$ (geikielite) at high temperatures and high pressures. American Mineralogist, 93, 39-47.

Palmer, S., Jagannadha Reddy, B., and Frost, R.L. (2007) Application of UV–Vis, near-infrared and mid-infrared spectroscopy to the study of Mn-bearing humites. Polyhedron, 26, 524-533.

Prasad, P.S.R., and Sarma, L.P. (2004) A near-infrared spectroscopic study of hydroxyl in natural chondrodite. American Mineralogist, 89, 1056-1060.

Qin, F., Wu, X., Zhang, D., Qin, S., and Jacobsen, S.D. (2017) Thermal equation of state of natural Ti-bearing clinohumite. Journal of Geophysical Research: Solid Earth, 122, 8943-8951.

Ribbe, P.H. (1979) Titanium, fluorine, and hydroxyl in the humite minerals. American Mineralogist, 64, 1027-1035.

Ribbe, P.H., and Gibbs, G.V. (1971) Crystal structures of the humite minerals: III. Mg/Fe ordering in humite and its relation to other ferromagnesian silicates. American Mineralogist, 56, 1155-1173.

Robinson, K., Gibbs, G.V., and Ribbe, P.H. (1973) The crystal structure of the humite

Always consult and cite the final, published document. See http:/www.minsocam.org or GeoscienceWorld

This is the peer-reviewed, final accepted version for American Mineralogist, published by the Mineralogical Society of America.
The published version is subject to change. Cite as Authors (Year) Title. American Mineralogist, in press.
DOI: https://doi.org/10.2138/am-2021-7538. http://www.minsocam.org/

minerals. IV. Clinohumite and Titanoclinohumite. American Mineralogist, 58, 43-49.

Rywak, A.A., and Burlitch, J.M. (1996) The crystal chemistry and thermal stability of sol-gel prepared fluoride-substituted talc. Physics and Chemistry of Minerals, 23, 418-431.

Scambelluri, M., and Rampone, E. (1999) Mg-metasomatism of oceanic gabbros and its control on Ti-clinohumite formation during eclogitization. Contributions to Mineralogy and Petrology, 135, 1-17.

Scambelluri, M., and Phillippot, P. (2001) Deep fluids in subduction zones. Lithos, 55, 213-227.

Shannon, R. D. (1976) Revised effective ionic radii and systematic studies of interatomic distances in halides and chalcogenides. Acta Crystallographica, A32, 751–767.

Sheldrick, G.M. (2008) A short history of SHELX. Acta Crystallographica, A64, 112-122.

Shen, T., Hermann, J., Zhang, L., Padrón-Navarta, J.A., and Chen, J. (2014) FTIR spectroscopy of Ti-chondrodite, Ti-clinohumite, and olivine in deeply subducted serpentinites and implications for the deep water cycle. Contributions to Mineralogy and Petrology, 167, 992, doi: 10.1007/s00410-014-0992-8.

Always consult and cite the final, published document. See http:/www.minsocam.org or GeoscienceWorld

This is the peer-reviewed, final accepted version for American Mineralogist, published by the Mineralogical Society of America.
The published version is subject to change. Cite as Authors (Year) Title. American Mineralogist, in press.
DOI: https://doi.org/10.2138/am-2021-7538. http://www.minsocam.org/

Shen, T., Hermann, J., Zhang, L., Lü, Z., Padrón-Navarta, J.A., Xia, B., and Bader, T. (2015) UHP metamorphism documented in Ti-chondrodite- and Ti-clinohumite-bearing serpentinized ultramafic rocks from Chinese southwestern Tianshan. Journal of petrology, 56, 1425-1458.

Smith, J.V., Delaney, J.S., Hervig, R.L., and Dawson, J.B. (1981) Storage of F and Cl in the upper mantle: geochemical implications. Lithos, 14, 133-147.

Smyth, J.R., Frost, D.J., Nestola, F., Holl, C.M., and Bromiley, G. (2006) Olivine hydration in the deep upper mantle: Effects of temperature and silica activity. Geophysical Research Letters, 33, L15301, doi: 10.1029/2006GL026194

Stalder, R., and Ulmer, P. (2001) Phase relations of a serpentine composition between 5 and 14 GPa: significance of clinohumite and phase E as water carriers into the transition zone. Contributions to Mineralogy and Petrology, 140, 670-679.

Tokonami, M. (1965) Atomic scattering factor for O^{2-}. Acta Crystallographica, 19, 486.

Trittschack, R., Grobéty, B., and Koch-Müller, M. (2012) In situ high-temperature Raman and FTIR spectroscopy of the phase transformation of lizardite. American Mineralogist, 97, 1965-1976.

Williams, Q. (1992) A vibrational spectroscopic study of hydrogen in high pressure mineral assemblages. In Syono Y. and Manghnani M. H., Eds., Geophysical

Always consult and cite the final, published document. See http:/www.minsocam.org or GeoscienceWorld

This is the peer-reviewed, final accepted version for American Mineralogist, published by the Mineralogical Society of America.
The published version is subject to change. Cite as Authors (Year) Title. American Mineralogist, in press.
DOI: https://doi.org/10.2138/am-2021-7538. http://www.minsocam.org/

Monograph Series, 67, p. 289-296. American Geophysical Union, Washington, D. C.

Wunder, B. (1998) Equilibrium experiments in the system $MgO–SiO_2–H_2O$ (MSH): stability fields of clinohumite-OH [$Mg_9Si_4O_{16}(OH)_2$], chondrodite-OH [$Mg_5Si_2O_8(OH)_2$] and phase A ($Mg_7Si_2O_8(OH)_6$). Contributions to Mineralogy and Petrology, 132, 111-120.

Wunder, B., Medenbach, O., Daniels, P., and Schreyer, W. (1995) First synthesis of the hydroxyl end-member of humite, $Mg_7Si_3O_{12}(OH)_2$. American Mineralogist, 80, 638-640.

Yang, Y., Wang, Z.P., Smyth, J.R., Liu, J., and Xia, Q.K. (2015) Water effects on the anharmonic properties of forsterite. American Mineralogist, 100, 2185-2190.

Yang, Y., Ingrin, J., Xia, Q., and Liu, W. (2019). Nature of hydrogen defects in clinopyroxenes from room temperature up to 1000℃: Implication for the preservation of hydrogen in the upper mantle and impact on electrical conductivity. American Mineralogist, 104, 79-93.

Ye, Y., Smyth, J.R., Jacobsen, S.D., and Goujon, C. (2013) Crystal chemistry, thermal expansion, and Raman spectra of hydroxyl-clinohumite: implications for water in Earth's interior. Contributions to Mineralogy and Petrology, 165, 563-574.

Ye, Y., Jacobsen, S.D., Mao, Z., Duffy, T.S., Hirner, S.M., and Smyth, J.R. (2015)

Always consult and cite the final, published document. See http:/www.minsocam.org or GeoscienceWorld

This is the peer-reviewed, final accepted version for American Mineralogist, published by the Mineralogical Society of America.
The published version is subject to change. Cite as Authors (Year) Title. American Mineralogist, in press.
DOI: https://doi.org/10.2138/am-2021-7538. http://www.minsocam.org/

Crystal structure, thermal expansivity, and elasticity of OH-chondrodite: trends among dense hydrous magnesium silicates. Contributions to Mineralogy and Petrology, 169, 43, doi: 10.1007/s00410-015-1138-3.

Zhang, M., Hui, Q., Lou, X.J., Redfern, S.A.T., Salje, E.K.H., and Tarantino, S.C. (2006) Dehydroxylation, proton migration, and structural changes in heated talc: an infrared spectroscopic study. American Mineralogist, 91, 816-825.

Zhu, X., Guo, X., Smyth, J. R., Ye, Y., Wang, X., and Liu, D. (2019). High-temperature vibrational spectra between Mg $(OH)_2$ and Mg $(OD)_2$: anharmonic contribution to thermodynamics and D/H fractionation for brucite. Journal of Geophysical Research: Solid Earth, 124, 8267-8280.

Always consult and cite the final, published document. See http:/www.minsocam.org or GeoscienceWorld

This is the peer-reviewed, final accepted version for American Mineralogist, published by the Mineralogical Society of America.
The published version is subject to change. Cite as Authors (Year) Title. American Mineralogist, in press.
DOI: https://doi.org/10.2138/am-2021-7538. http://www.minsocam.org/

Figure captions

Figure 1 Crystal structures of **(a)** humite and **(b)** norbergite, viewed approximately in the ***b*** and ***a*** directions, respectively. The protons are shown as small white spheres, and the covalent O-H bonds are presented as short black lines. The OH...OH distances are plotted in **(c)** for humite and in **(d)** for norbergite, viewed approximately in ***a*** direction. H-H repulsion in humite is also illustrated in **(c)**.

Figure 2 Selected Raman spectra of the lattice vibrations of natural **(a)** humite and **(b)** norbergite at various temperatures with the background subtracted. The peak positions are indicated for the spectra obtained at 300 K, and the intensities of the weak bands below 700 cm^{-1} are magnified by 4 times for clarity.

Figure 3 Temperature dependence of the Raman-active modes for both the natural humite (black) and norbergite (gray) samples with a linear regression for each vibration in the frequency ranges of **(a)** 100-400 cm^{-1}, **(b)** 400-800 cm^{-1} and **(c)** 800-1000 cm^{-1}. The peak positions at 293 K are labeled at the left sides of the figures. The uncertainties for the fitted peak positions are smaller than the sizes of the symbols.

Always consult and cite the final, published document. See http:/www.minsocam.org or GeoscienceWorld

This is the peer-reviewed, final accepted version for American Mineralogist, published by the Mineralogical Society of America.
The published version is subject to change. Cite as Authors (Year) Title. American Mineralogist, in press.
DOI: https://doi.org/10.2138/am-2021-7538. http://www.minsocam.org/

Figure 4 FTIR and Raman spectra of the OH-stretching modes of natural **(a)** clinohumite, **(b)** humite and **(c)** norbergite under ambient condition, with the peak positions labeled.

Figure 5 Representative FTIR **(a, b)** and Raman **(c, d)** spectra for the OH-stretching modes of the natural humite **(a, c)** and norbergite **(b, d)** samples at high temperatures.

Figure 6 Temperature dependence of the OH bands for both the natural **(a)** humite and **(b)** norbergite samples with linear regressions. The IR-active and Raman-active modes are indicated by solid and open symbols, respectively, and the frequencies at room temperature are also listed in the figures. The uncertainties for the fitted peak positions are smaller than the sizes of the symbols.

Figure 7 Temperature dependence of the OH-stretching modes, $(\partial v_i/\partial T)_P$, for the DHMS phases in the hydrous peridotite system (a: this study; b: Liu et al. 1999; c: Liu et al. 2019a; d: Lin et al. 2000; e: Lin et al. 1999; f: Liu et al. 1997b; g: Liu et al. 1997a; h: Liu et al. 1998; i: Liu et al. 2002; j: Zhang et al. 2006; k: Zhu et al. 2019; l: Liu et al. 2019b; m: Trittschack et al. 2012).

Always consult and cite the final, published document. See http:/www.minsocam.org or GeoscienceWorld

This is the peer-reviewed, final accepted version for American Mineralogist, published by the Mineralogical Society of America.
The published version is subject to change. Cite as Authors (Year) Title. American Mineralogist, in press.
DOI: https://doi.org/10.2138/am-2021-7538. http://www.minsocam.org/

Figure 8(a-c) Ratios of the integral intensities for OH-stretching modes in the frequency ranges below and above 3450 cm^{-1}, $I_{<3450}$: $I_{>3450}$. The intensity ratios for the IR-active modes are plotted as a function of the **(a)** fluorine or **(b)** titanium concentration, while the intensity ratios for the Raman-active modes are plotted as a function of the **(c)** titanium content. (clinohumite: Frost et al. 2007, Koga et al. 2014, Shen et al. 2014, Liu et al. 2019a; chondrodite: Williams 1992, Cynn et al. 1996, Kuribayashi et al. 2004, Shen et al. 2014; humite and norbergite: this study). X_F is the ratio F/(F+OH), and X_{Ti} is the fraction of Ti at the M3 sites (Please refer to **Appendix Table 3** for more details).

Figure 9 Comparison of the isobaric mode Grüneisen parameters for the humite-group minerals on the brucite-forsterite join (humite and norbergite: this study; chondrodite: Mernagh et al. 1999; clinohumite: Liu et al. 2019a; forsterite: Gillet et al. 1991; brucite: Zhu et al. 2019).

Always consult and cite the final, published document. See http:/www.minsocam.org or GeoscienceWorld

This is the peer-reviewed, final accepted version for American Mineralogist, published by the Mineralogical Society of America.
The published version is subject to change. Cite as Authors (Year) Title. American Mineralogist, in press.
DOI: https://doi.org/10.2138/am-2021-7538. http://www.minsocam.org/

Table 1. Electron microprobe analyses for the natural humite and norbergite samples.

	Humite	Norbergite		Humite	Norbergite
FeO (wt%)	6.88(1)	0.40(1)	Fe (apfu)	0.479(1)	0.011(0)
MgO	52.38(5)	58.15(5)	Mg	6.497(6)	2.968(3)
MnO	0.23(3)	0.02(1)	Mn	0.016(2)	0.001(0)
TiO_2	0.26(1)	0.99(3)	Ti	0.016(1)	0.025(1)
SiO_2	35.95(6)	29.05(5)	Si	2.991(5)	0.994(2)
F	2.50(5)	11.33(8)	F	0.658(5)	1.227(9)
Total[a]	97.15	95.17	H	1.310	0.722
H_2O[b]	2.36	3.16			

a: Measured total weight percentages without H_2O.

b: The formula of the humite-group minerals can be expressed as $n Mg_2SiO_4 \cdot Mg_{1-x}Ti_xO_{2x}(F,OH)_{2-2x}$, where n = 1 for norbergite, and n = 3 for humite. The weight percentages of H_2O were calculated assuming that the molar ratio of (H+F+2·Ti) : (O+F) was 2 : 14 for humite and 2 : 6 for norbergite.

Always consult and cite the final, published document. See http:/www.minsocam.org or GeoscienceWorld

This is the peer-reviewed, final accepted version for American Mineralogist, published by the Mineralogical Society of America.
The published version is subject to change. Cite as Authors (Year) Title. American Mineralogist, in press.
DOI: https://doi.org/10.2138/am-2021-7538. http://www.minsocam.org/

Appendix Table 1. Frequencies of the lattice vibrations (ν_i), the temperature dependence and the isobaric mode Grüneisen parameters.

Humite			Norbergite		
ν_i (cm^{-1})	$(\partial\nu_i/\partial T)_P$ (cm^{-1}/K)	γ_{iP}	ν_i (cm^{-1})	$(\partial\nu_i/\partial T)_P$ (cm^{-1}/K)	γ_{iP}
153	-0.013(3)	2.331(1)	199	-0.012(9)	1.654(9)
193	-0.022(3)	3.098(5)	225	-0.022(5)	2.553(1)
204	-0.018(9)	2.484(5)	257	-0.022(2)	2.185(4)
274	-0.012(7)	1.243(1)	290	-0.016(9)	1.487(8)
325	-0.021(2)	1.749(3)	329	-0.020(4)	1.583(1)
356	-0.027(1)	2.033(9)	380	-0.026(2)	1.760(2)
384	-0.010(2)	0.712(3)	429	-0.021(8)	1.297(3)
432	-0.023(5)	1.458(8)	489	-0.016(5)	0.861(4)
467	-0.029(4)	1.688(3)	517	-0.008(2)	0.404(9)
502	-0.034(1)	1.821(6)	555	-0.010(7)	0.492(2)
538	-0.005(3)	0.264(2)	573	-0.009(7)	0.432(2)
578	-0.022(1)	1.025(3)	611	-0.018(1)	0.756(3)
604	-0.016(8)	0.745(9)	770	-0.042(2)	1.399(2)
755	0.0002(1)	-0.007(1)	792	-0.009(9)	0.319(1)
783	-0.007(8)	0.267(1)	851	-0.014(9)	0.447(1)

Always consult and cite the final, published document. See http:/www.minsocam.org or GeoscienceWorld

This is the peer-reviewed, final accepted version for American Mineralogist, published by the Mineralogical Society of America.
The published version is subject to change. Cite as Authors (Year) Title. American Mineralogist, in press.
DOI: https://doi.org/10.2138/am-2021-7538. http://www.minsocam.org/

843	-0.014(7)	0.467(6)	885	-0.026(2)	0.755(8)
865	-0.005(8)	0.179(8)	894	-0.020(3)	0.579(7)
932	-0.026(1)	0.751(1)	951	-0.023(1)	0.620(1)
968	-0.025(6)	0.709(2)	973	-0.035(2)	0.923(6)

Always consult and cite the final, published document. See http:/www.minsocam.org or GeoscienceWorld

This is the peer-reviewed, final accepted version for American Mineralogist, published by the Mineralogical Society of America.
The published version is subject to change. Cite as Authors (Year) Title. American Mineralogist, in press.
DOI: https://doi.org/10.2138/am-2021-7538. http://www.minsocam.org/

Appendix Table 2. Frequencies of the OH-stretching vibrations, the temperature dependence and the isobaric mode Grüneisen parameters.

Mineral	ν_i (cm^{-1})	$(\partial \nu_i/\partial T)_P$ (cm^{-1}/K)	γ_{iP}
Norbergite	3582[a]	-0.023(7)	0.168(9)
	3315[b]	0.023(1)	-0.177(9)
	3365[b]	0.023(9)	-0.181(3)
	3581[b]	-0.025(9)	0.184(6)
	3665[b]	-0.043(9)	0.305(8)
Humite	3390[a]	0.010(9)	-0.086(2)
	3556[a]	-0.014(6)	0.110(1)
	3568[a]	-0.013(6)	0.102(2)
	3333[b]	0.026(9)	-0.216(4)
	3381[b]	0.024(8)	-0.196(7)
	3556[b]	-0.047(2)	0.355(9)
	3573[b]	-0.028(2)	0.210(2)
Clinohumite	3310[a]	0.053(1)	-0.458(6)
	3405[a]	0.018(8)	-0.158(3)
	3528[a]	-0.025(2)	0.204(9)
	3565[a]	-0.022(7)	0.182(6)

Always consult and cite the final, published document. See http:/www.minsocam.org or GeoscienceWorld

3309[b]	0.015(8)	-0.136(8)
3397[b]	0.021(8)	-0.183(8)
3529[b]	-0.027(6)	0.224(1)
3564[b]	-0.022(9)	0.184(1)
3608[b]	-0.041(7)	0.331(1)

a: Raman-active OH bands; b: IR-active OH bands.

Always consult and cite the final, published document. See http:/www.minsocam.org or GeoscienceWorld

This is the peer-reviewed, final accepted version for American Mineralogist, published by the Mineralogical Society of America.
The published version is subject to change. Cite as Authors (Year) Title. American Mineralogist, in press.
DOI: https://doi.org/10.2138/am-2021-7538. http://www.minsocam.org/

Appendix Table 3. Raman and infrared measurements for humite-group minerals with various fluorine and titanium concentrations under ambient condition. The integral intensities below and above 3450 cm^{-1} are estimated from the reported spectra.

Mineral	X_{Ti}	X_F	$I_{<3450}/I_{>3450}$	Reference
F-rich ($X_F \geq 0.33$) samples by **FTIR** measurements (**Fig. 7a**)				
Chondrodite	0.05	0.73	0.47(5)	Williams (1992)
Chondrodite	0.02	0.88	0.25(3)	Cynn et al. (1996)
Chondrodite	0.02	0.37	0.42(4)	Kuribayashi et al. (2004)
Humite	0.016	0.33	0.43(2)	This study
Norbergite	0.03	0.63	0.85(3)	--
Ti-rich ($X_{Ti} \geq 0.08$) samples by **FTIR** measurements (**Fig. 7b**)				
Clinohumite	0.45	0	4.81(5)	Shen et al. (2014)
Clinohumite	0.33	0	3.36(3)	--
Clinohumite	0.18	0	2.45(2)	--
Chondrodite	0.36	0	5.21(5)	--
Chondrodite	0.29	0	3.92(4)	--
Clinohumite	0.25	0.13	2.97(1)	Liu et al. (2019a)
Clinohumite	0.45	0.01	7.31(7)	Koga et al. (2014)
Clinohumite	0.43	0.01	7.12(7)	--

Always consult and cite the final, published document. See http:/www.minsocam.org or GeoscienceWorld

This is the peer-reviewed, final accepted version for American Mineralogist, published by the Mineralogical Society of America.
The published version is subject to change. Cite as Authors (Year) Title. American Mineralogist, in press.
DOI: https://doi.org/10.2138/am-2021-7538. http://www.minsocam.org/

Clinohumite	0.46	0.01	9.75(9)	--
Clinohumite	0.41	0.14	4.11(4)	--
Clinohumite	0.39	0.17	3.26(3)	--
Ti-rich ($X_{Ti} \geq 0.08$) samples by **Raman** measurements (**Fig. 7c**)				
Clinohumite	0.08	0	0.92(9)	Frost et al. (2007)
Clinohumite	0.21	0	1.16(9)	Frost et al. (2007)
Clinohumite	0.25	0.2	1.29(1)	Liu et al. (2019a)
Clinohumite	0.46	0.01	4.14(4)	Koga et al. (2014)
Clinohumite	0.43	0.01	3.25(3)	--
Clinohumite	0.39	0.17	1.16(9)	--
Clinohumite	0.41	0.14	6.75(7)	--

X_F is F/(F+OH) in moles. X_{Ti} is the fraction of Ti at the M3 site.

Always consult and cite the final, published document. See http:/www.minsocam.org or GeoscienceWorld

Figure 1

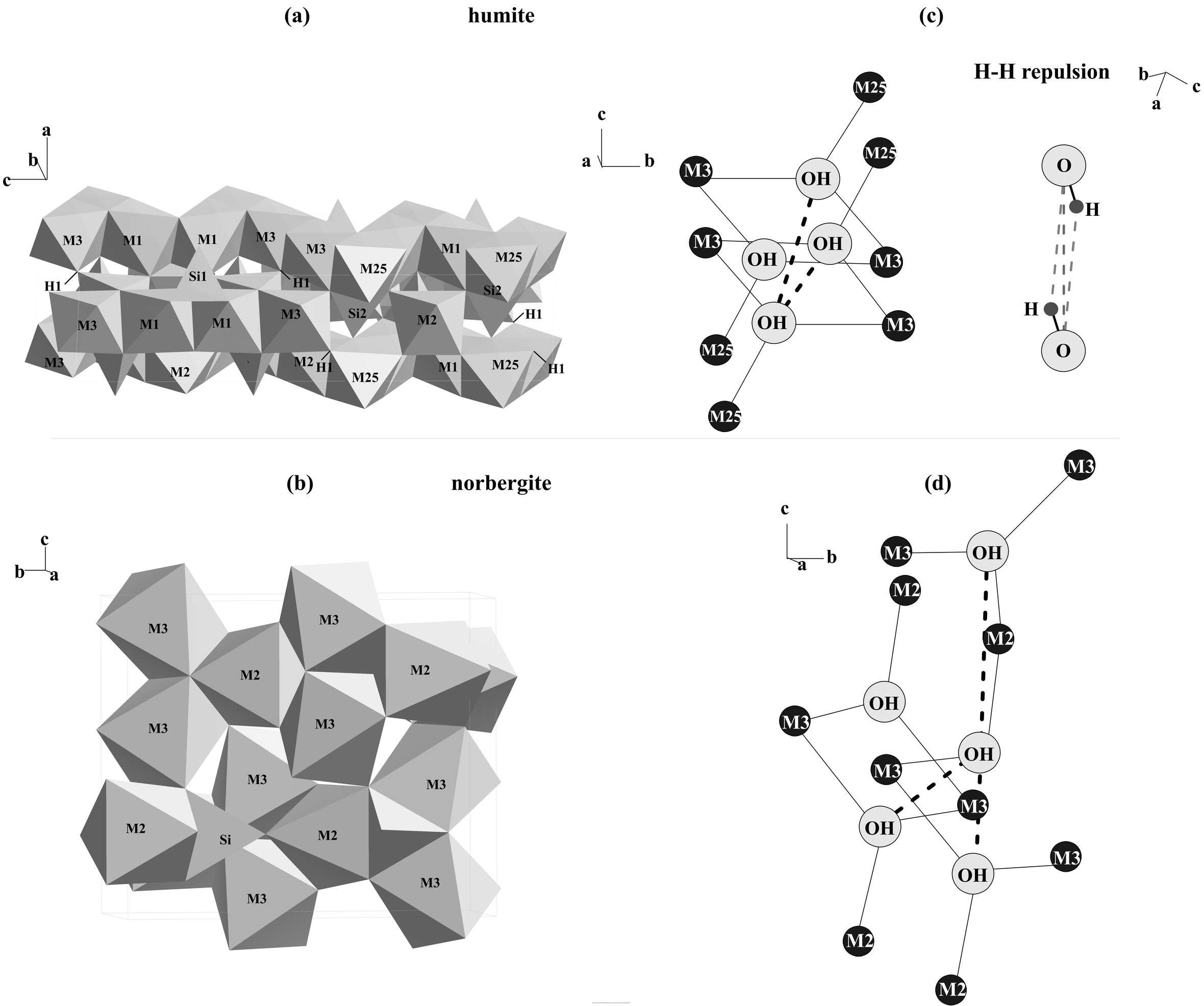
(a)
humite
a
b
c
M3
M1
M1
M3
M3
M25
M1
M25
H1
Si1
H1
Si2
H1
M3
M1
M1
M3
Si2
M2
M3
M2
M2
H1
M25
M1
M25
H1
(c)
H-H repulsion
b
c
a
c
a
b
M25
M25
M3
OH
M3
OH
OH
M3
OH
M3
M25
M25
O
H
H
O
(b)
norbergite
c
b
a
M3
M3
M2
M2
M3
M3
M3
M3
M2
Si
M2
M3
M3
(d)
M3
c
b
a
M3
OH
M2
M2
OH
M3
OH
M3
M3
OH
M3
OH
M2
M2

This is the peer-reviewed, final accepted version for American Mineralogist, published by the Mineralogical Society of America.
The published version is subject to change. Cite as Authors (Year) Title. American Mineralogist, in press.
DOI: https://doi.org/10.2138/am-2021-7538. http://www.minsocam.org/

Figure 2

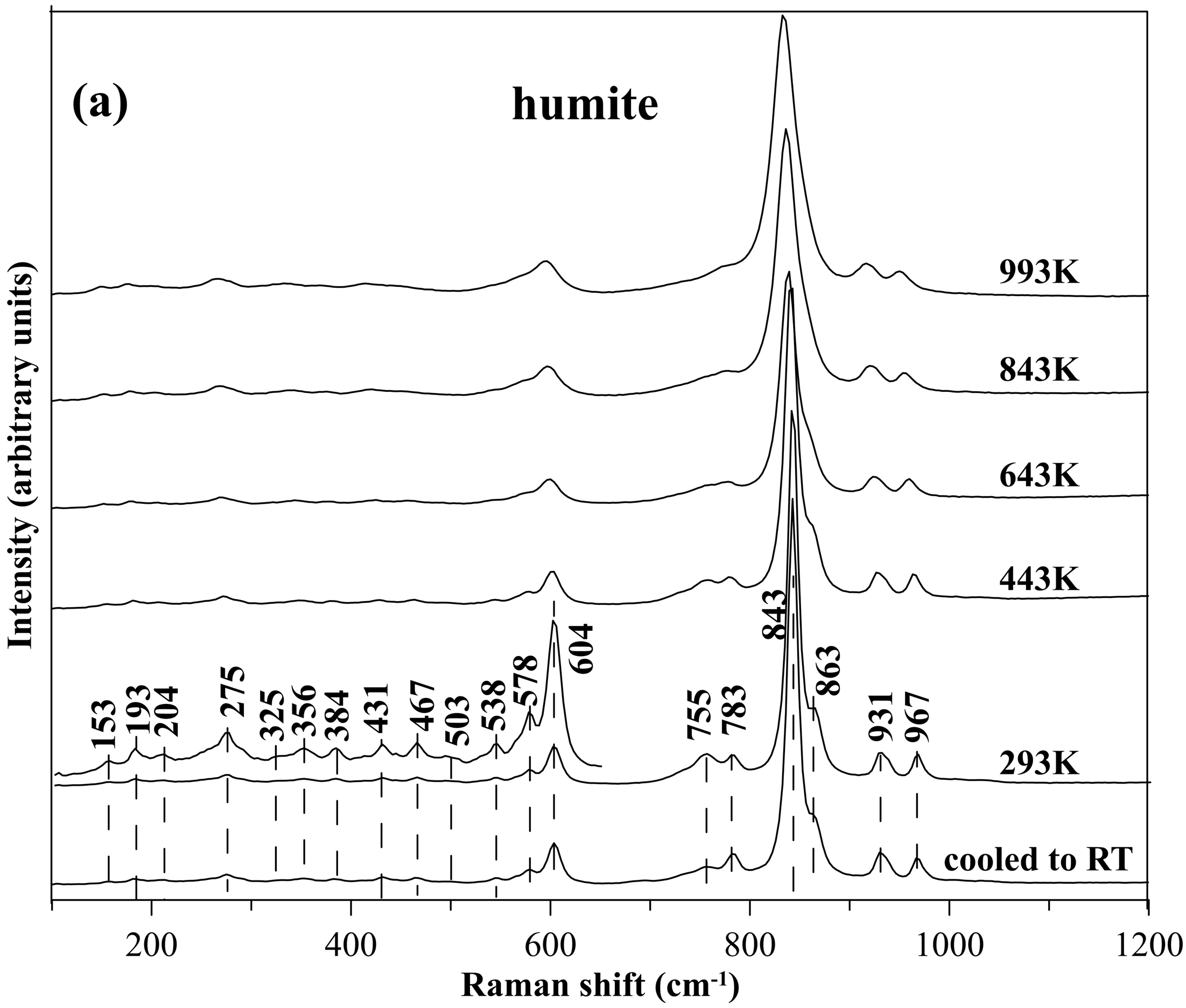

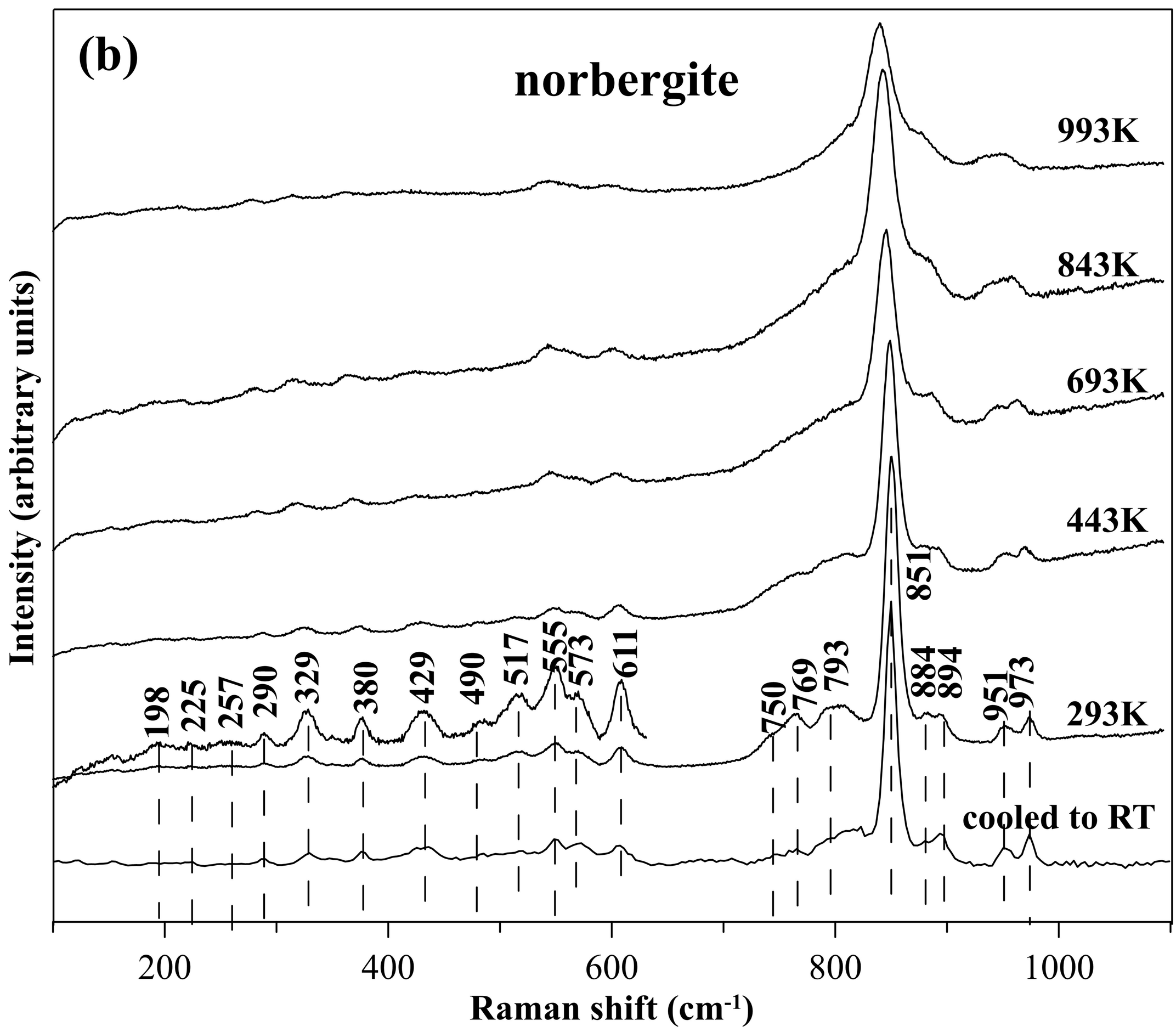

Always consult and cite the final, published document. See http:www.minsocam.org or GeoscienceWorld

Figure 3

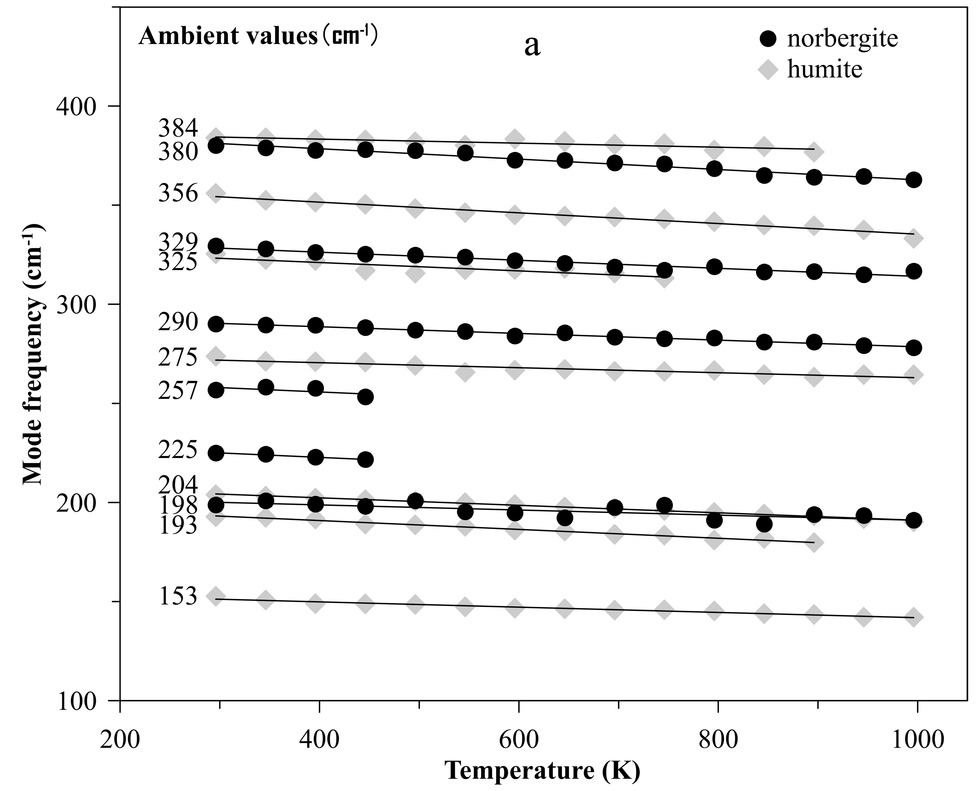
Ambient values (cm-1)
a
norbergite
humite
384
380
356
329
325
290
275
257
225
204
198
193
153
Mode frequency (cm-1)
Temperature (K)

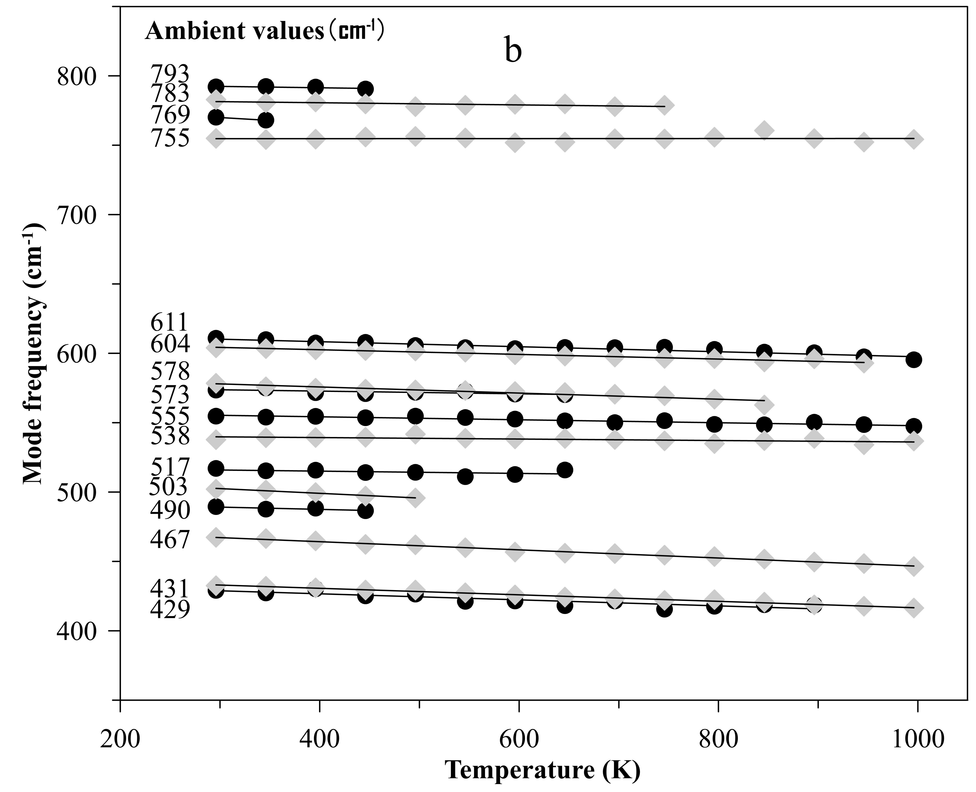
Ambient values (cm-1)
b
793
783
769
755
611
604
578
573
555
538
517
503
490
467
431
429
Mode frequency (cm-1)
Temperature (K)

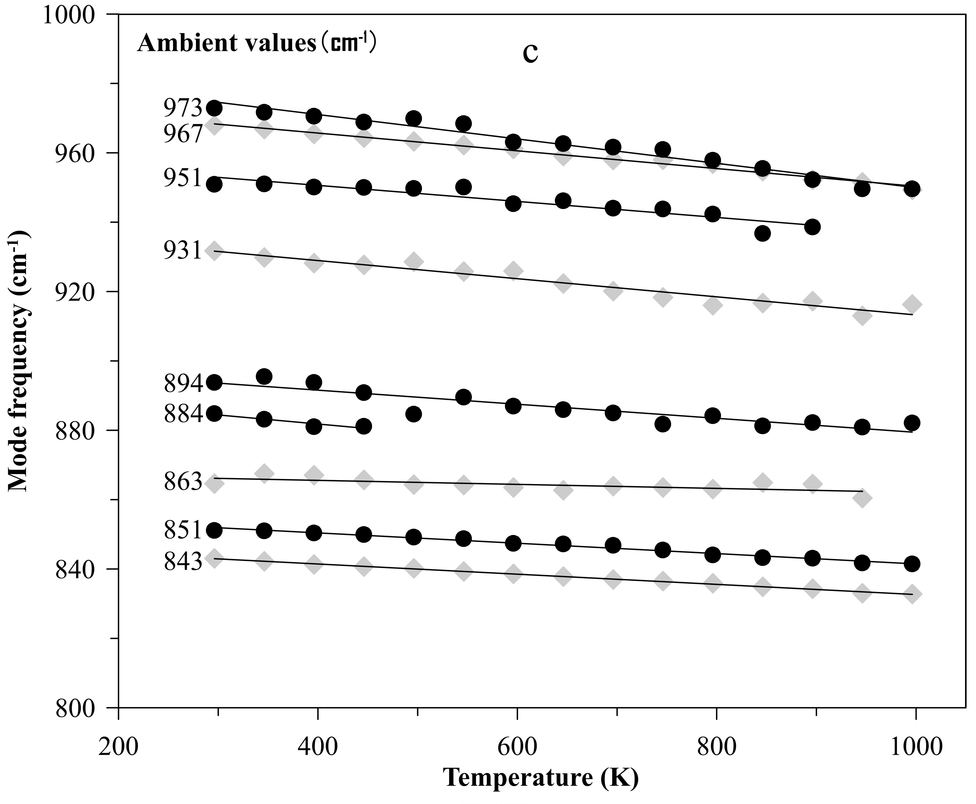
Ambient values (cm-1)
c
973
967
951
931
894
884
863
851
843
Mode frequency (cm-1)
Temperature (K)

This is the peer-reviewed, final accepted version for American Mineralogist, published by the Mineralogical Society of America.
The published version is subject to change. Cite as Authors (Year) Title. American Mineralogist, in press.
DOI: https://doi.org/10.2138/am-2021-7538. http://www.minsocam.org/

Figure 4

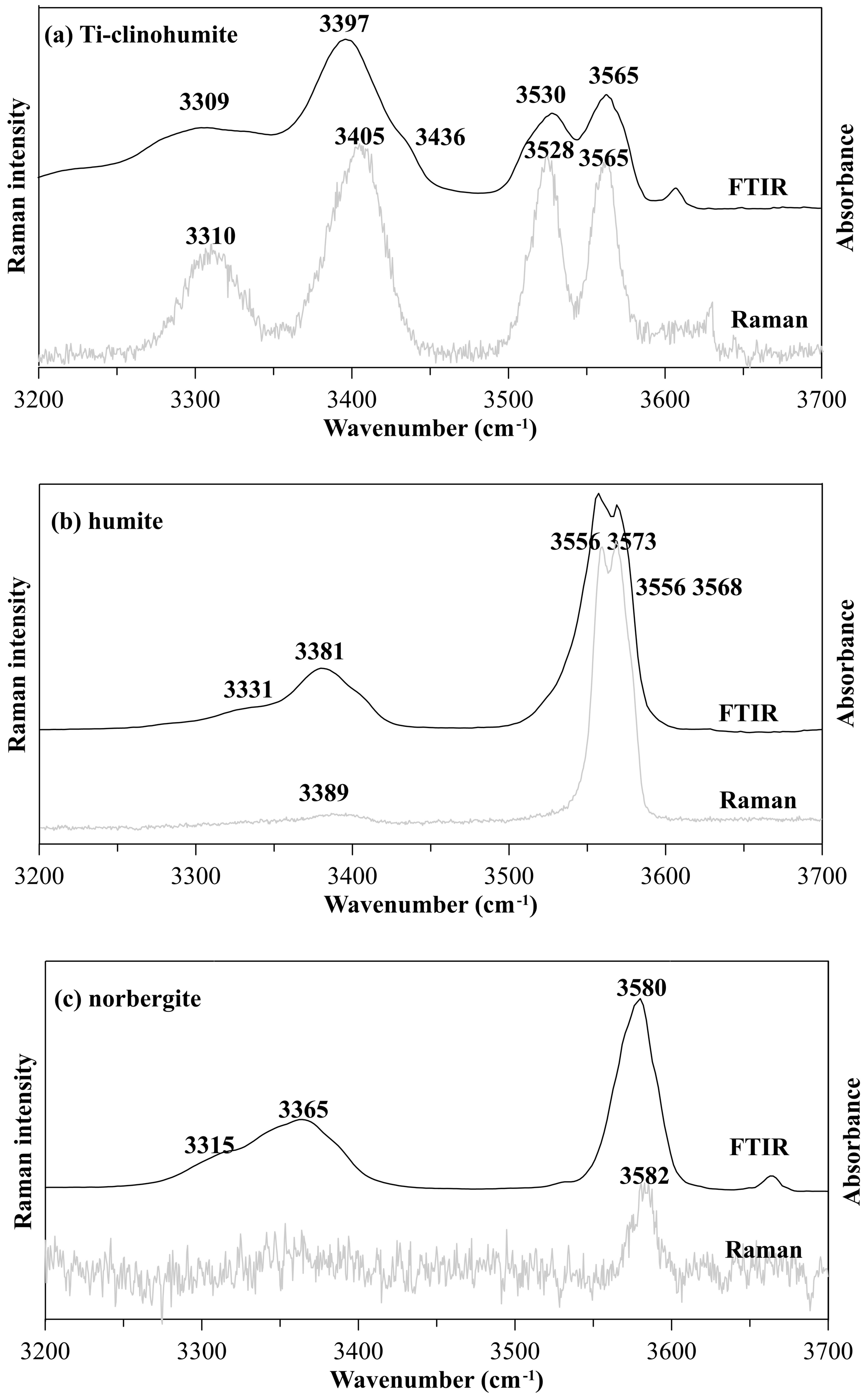

Always consult and cite the final, published document. See http:www.minsocam.org or GeoscienceWorld

Figure 5

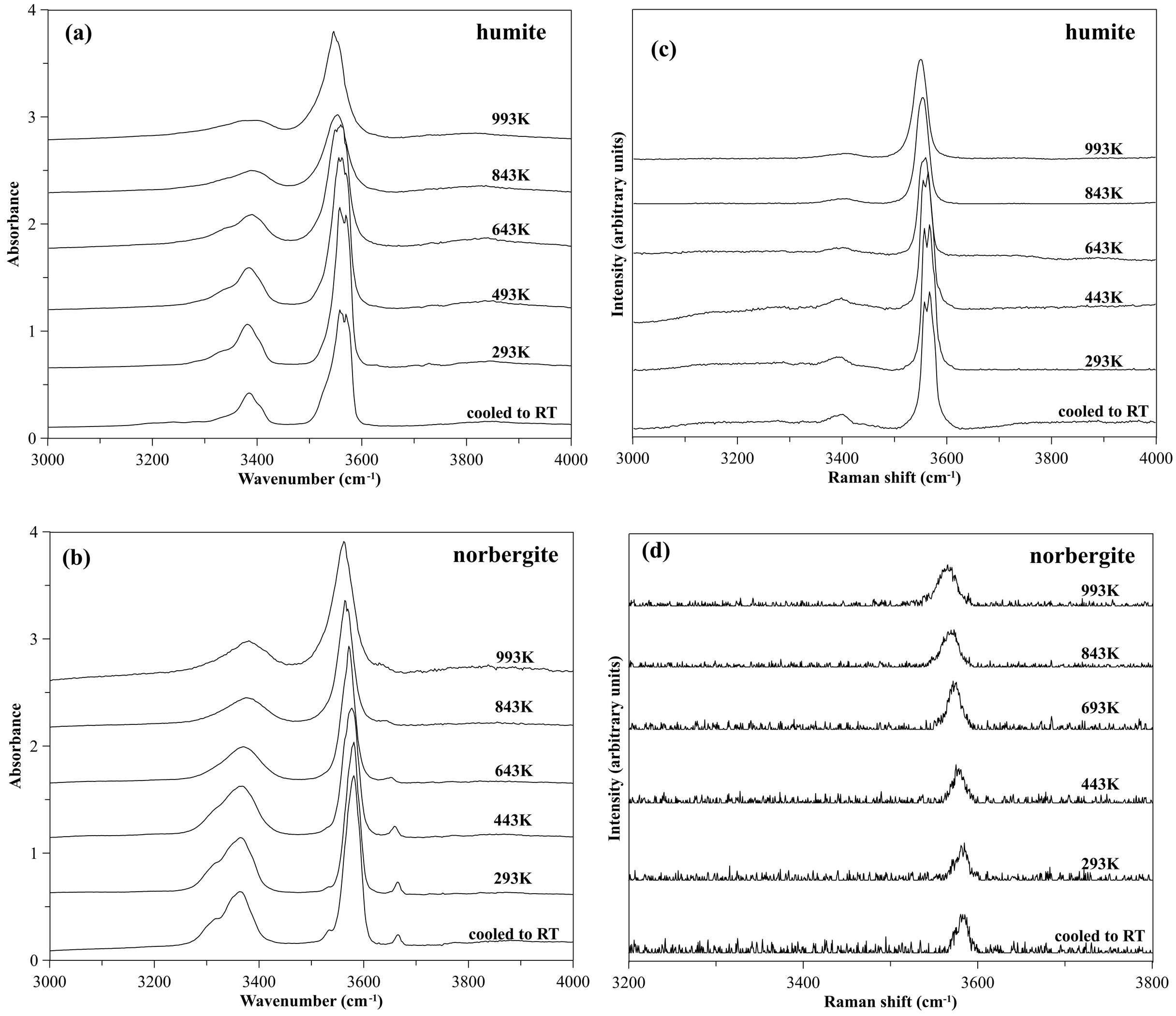
(a)
humite
993K
843K
643K
493K
293K
cooled to RT
Absorbance
Wavenumber (cm-1)
(c)
humite
993K
843K
643K
443K
293K
cooled to RT
Intensity (arbitrary units)
Raman shift (cm-1)
(b)
norbergite
993K
843K
643K
443K
293K
cooled to RT
Absorbance
Wavenumber (cm-1)
(d)
norbergite
993K
843K
693K
443K
293K
cooled to RT
Intensity (arbitrary units)
Raman shift (cm-1)

This is the peer-reviewed, final accepted version for American Mineralogist, published by the Mineralogical Society of America.
The published version is subject to change. Cite as Authors (Year) Title. American Mineralogist, in press.
DOI: https://doi.org/10.2138/am-2021-7538. http://www.minsocam.org/

Figure 6

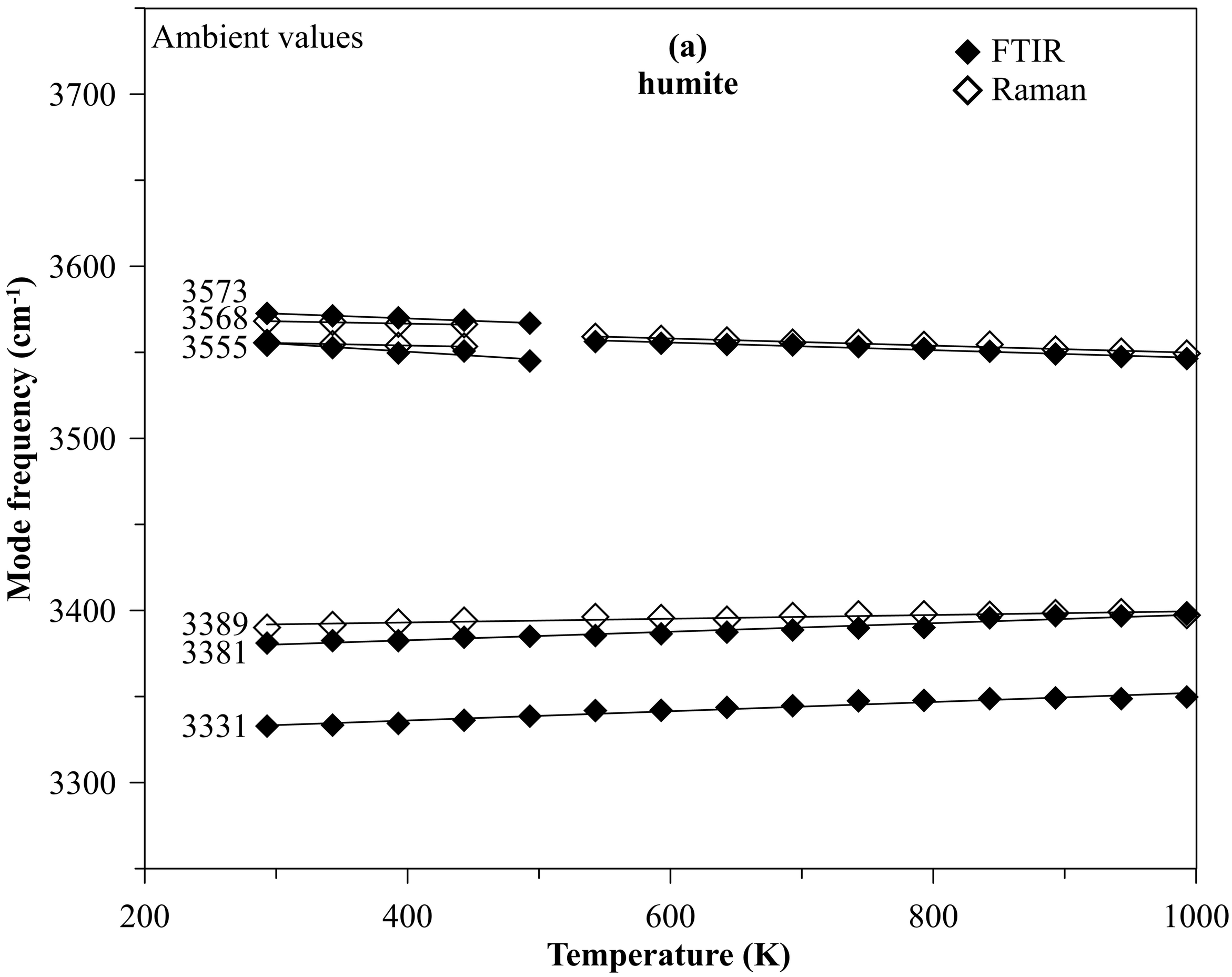

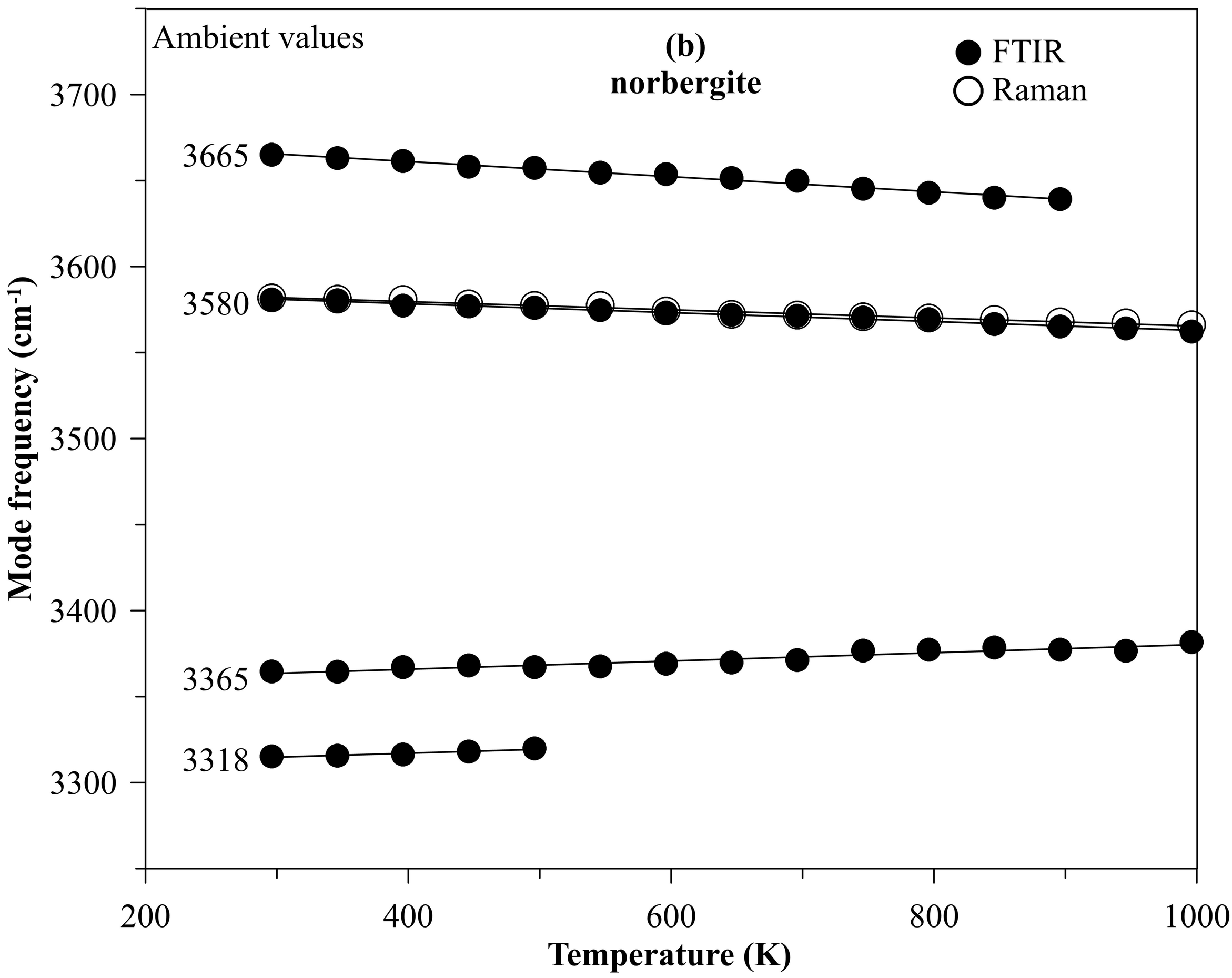

Always consult and cite the final, published document. See http:www.minsocam.org or GeoscienceWorld

This is the peer-reviewed, final accepted version for American Mineralogist, published by the Mineralogical Society of America.
The published version is subject to change. Cite as Authors (Year) Title. American Mineralogist, in press.
DOI: https://doi.org/10.2138/am-2021-7538. http://www.minsocam.org/

Figure 7

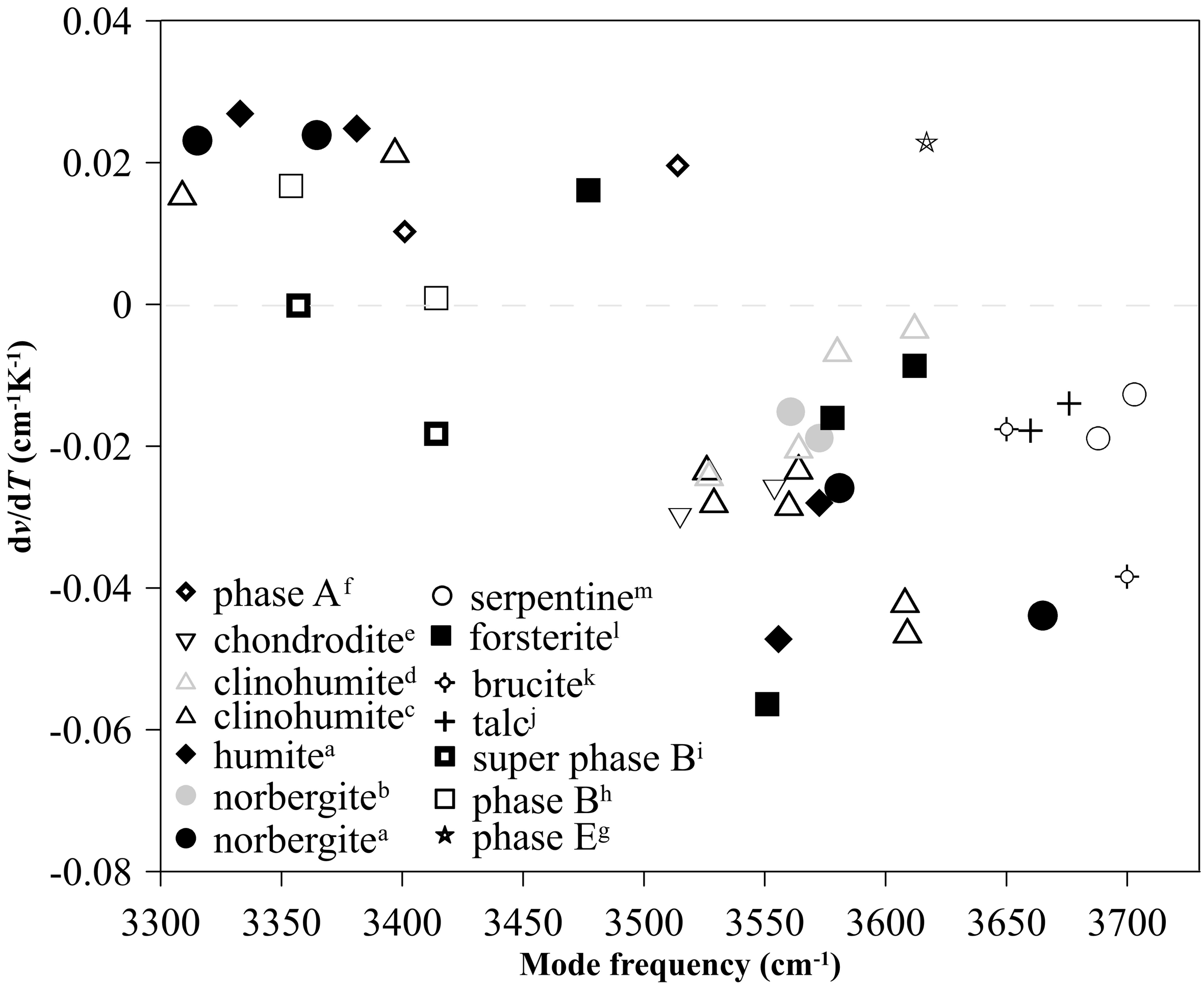

Always consult and cite the final, published document. See http:www.minsocam.org or GeoscienceWorld

This is the peer-reviewed, final accepted version for American Mineralogist, published by the Mineralogical Society of America.
The published version is subject to change. Cite as Authors (Year) Title. American Mineralogist, in press.
DOI: https://doi.org/10.2138/am-2021-7538. http://www.minsocam.org/

Figure 8

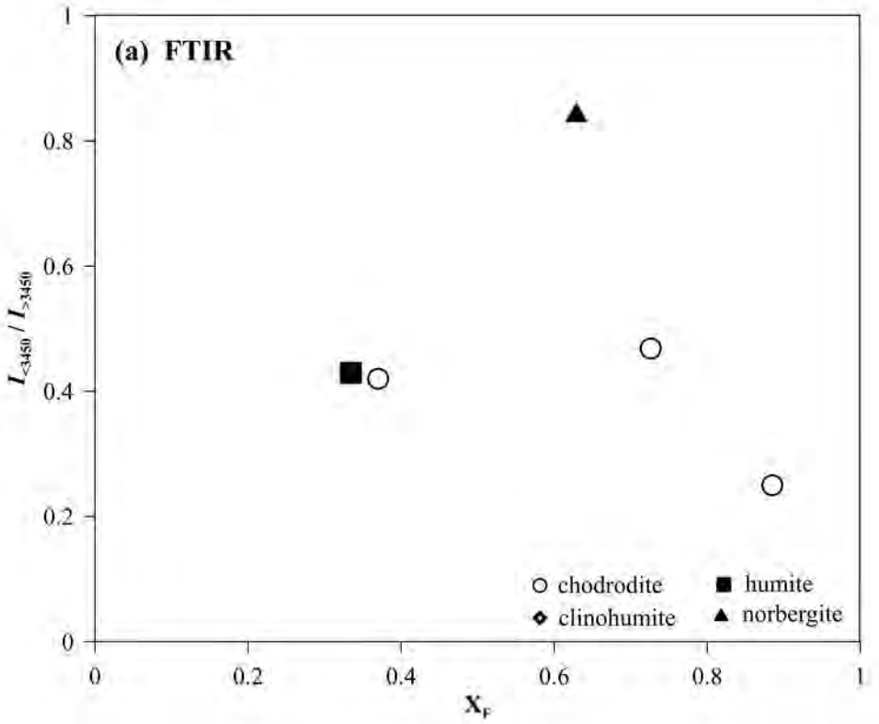

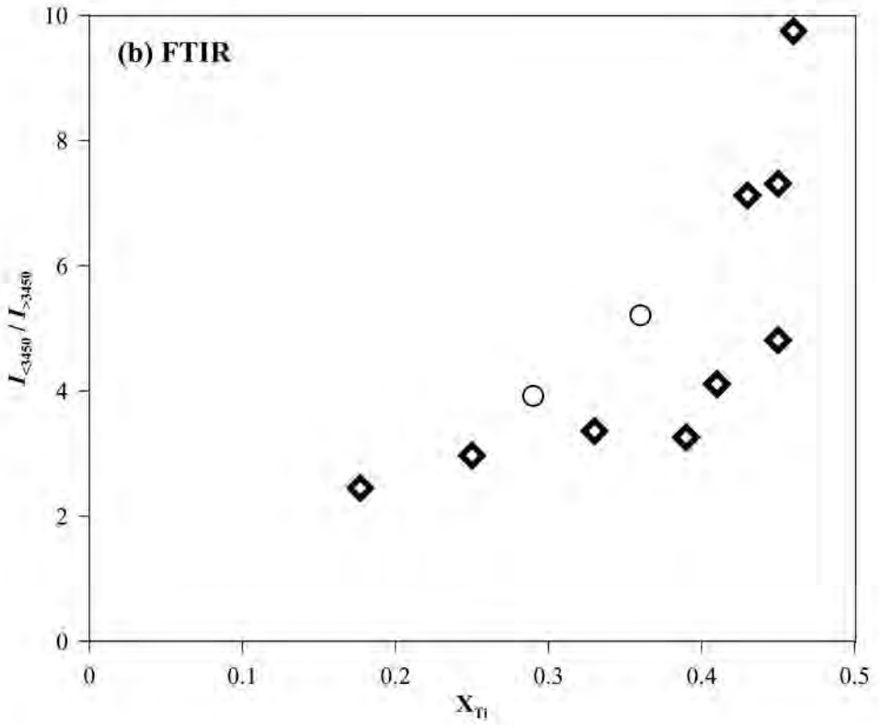

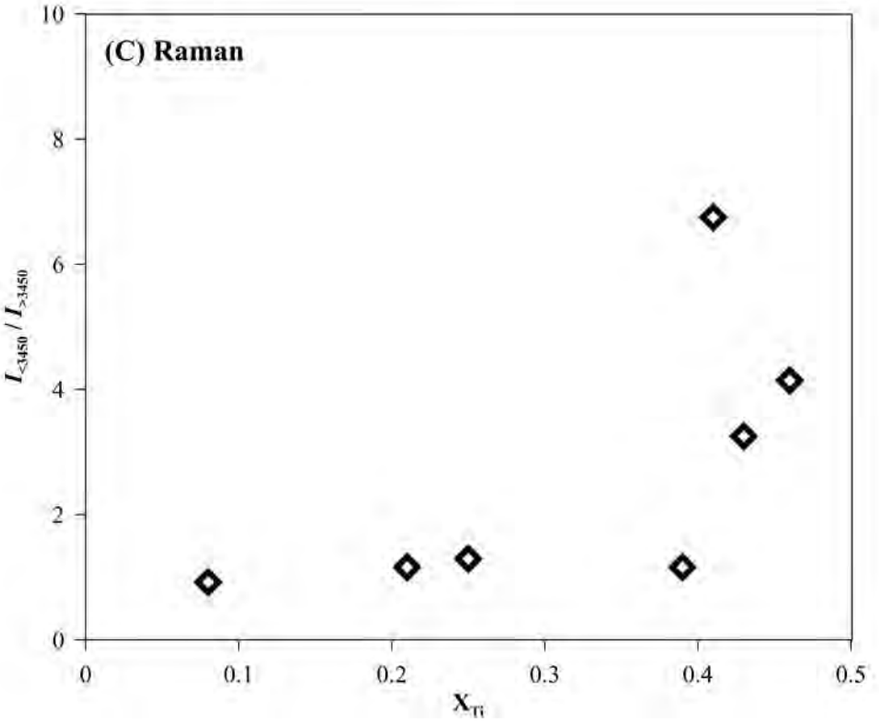

Always consult and cite the final, published document. See http:/www.minsocam.org or GeoscienceWorld

This is the peer-reviewed, final accepted version for American Mineralogist, published by the Mineralogical Society of America.
The published version is subject to change. Cite as Authors (Year) Title. American Mineralogist, in press.
DOI: https://doi.org/10.2138/am-2021-7536 , http://www.minsocam.org/

Figure 9

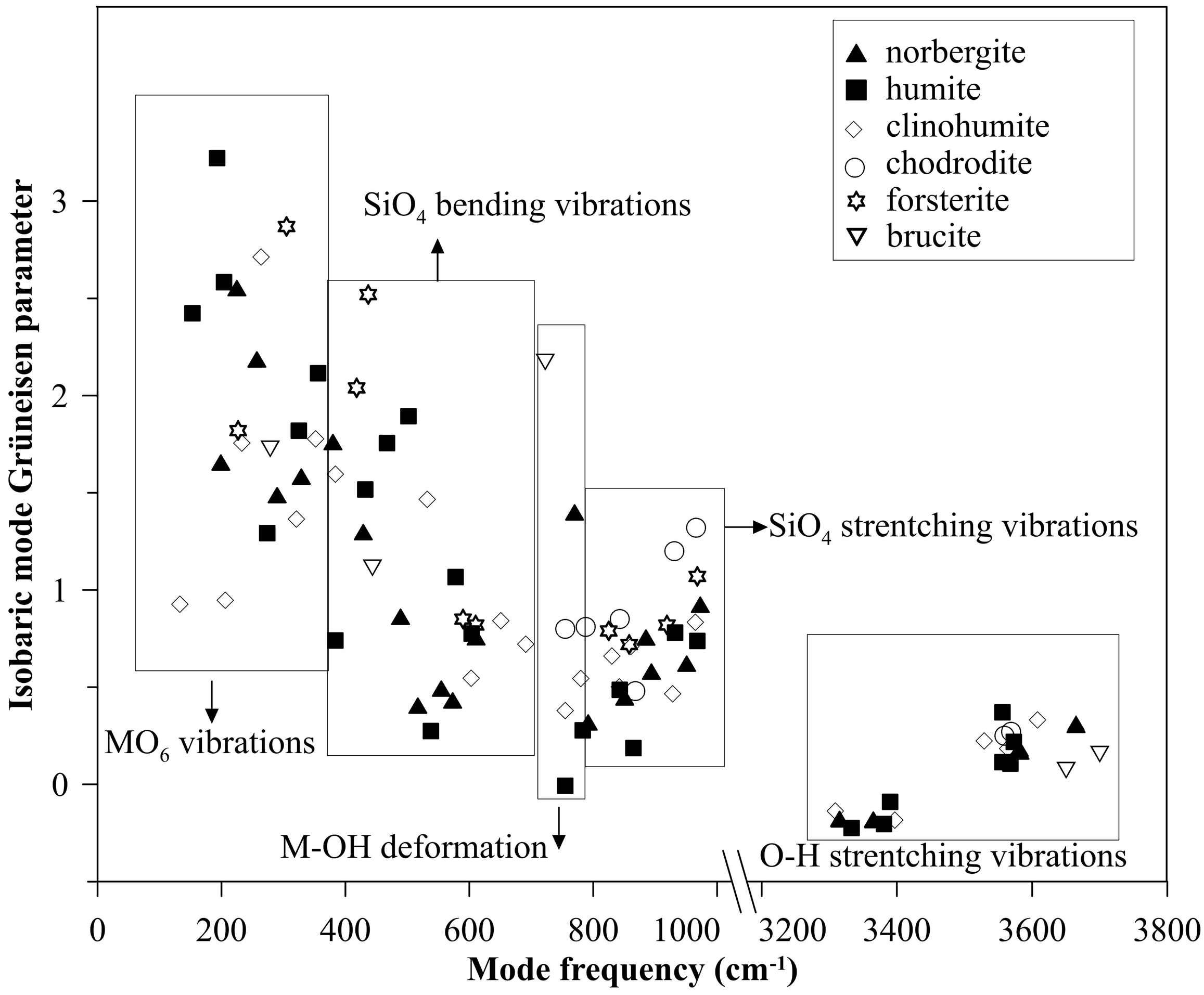

Always consult and cite the final, published document. See http://www.minsocam.org or GeoscienceWorld